USE OF COMPUTATIONAL FLUID DYNAMICS (CFD) TO MODEL FLOW AT PUMP INTAKES

by

Jennifer Anne Roberge

A Thesis

Submitted to the Faculty

of the

WORCESTER POLYTECHNIC INSTITUTE

in partial fulfillment of the requirements for the

Degree of Master of Science

in

Environmental Engineering

May 1999

APPROVED:

Dr. Paul P. Mathisen, Major Advisor

Dr. Frederick L. Hart, Head of Department

Abstract

This thesis presents a series of physical experiments and numerical simulations intended to determine whether the use of commercially available computational fluid dynamics (CFD) software may provide a viable alternative to the use of physical models for predicting the occurrence of vortices and swirl in pump intakes. The physical experiments were set up at Alden Research Laboratories, Inc. (ARL) of Holden, Massachusetts, using a simple pump intake model donated by ARL for use in this study. Swirl and velocity measurements and dye injections were used to characterize the flow in the physical model. Three flow conditions were chosen for the physical experiments because they demonstrated swirl and vortices developing at the pump intake.

Once the physical experiments were performed, FIDAP, a general-purpose finite-element CFD package, was used to simulate the circulation patterns in the vicinity of a pump intake. The model configuration and scale were selected to simulate experimental conditions in the physical pump intake model. Some similarities were also identified in the locations of the model's predicted vortex characteristics and the vortex characteristics that were observed in the experimental facility. However, the characteristics of swirl within the pump intake differed from experimental observations. Therefore, additional simulations were conducted to analyze the sensitivity of simulations to model assumptions. These additional simulations showed that the assumptions related to these model parameters have minor affects on the general nature of the predicted vortices, but do affect the predicted vortex strength. This thesis represents a first step in addressing the discrepancies between numerical and experimental results. Additional investigations are recommended to clarify the applicability of CFD to address pump intake problems.

Acknowledgements

I would like to thank Alden Research Laboratory, Inc. (ARL) and the staff of ARL for provided the model and for helping me when I needed assistance. Special thanks to Stuart Cain for answering all of my questions about FIDAP and Madadevan (Padu) Padmanabhan for coordinating the project. I would also like to thank William Durgin and George Hecker for providing the funding for this study.

Thank you to Dr. Paul Mathisen for advising the project and for helping me to set up and run the experiments.

I would also like to thank my parents whose faith and support helped me to finish the last six years of school.

Thank you to all of my friends who supported me, especially Jami Walsh for helping me to have some fun throughout last two years, and Troy Thompson for believing in me and for helping me to put my thesis together.

Contents

List of Figures

List of Tables

1.0 Introduction

1.1 Background/Problem Statement

Strong free surface and subsurface vortices often form in basins associated with pump intakes, navigation locks, and other hydraulic structures. These vortices can lead to swirl, reduced flow, air entrainment, and inefficient equipment operation (e.g. Padmanabhan and Hecker, 1984; Sweeney et. al., 1982). Despite extensive research efforts by numerous investigators, the processes in governing these vortices cannot be represented analytically. Therefore, designers and engineers commonly employ physical models to develop designs that prevent vortex problems in hydraulic structures. These physical models are site-specific and expensive to develop. Significant cost savings could be realized if the designs for pump intakes and other structures could be developed using computational fluid dynamics (CFD) models. Unfortunately, no known investigations have shown that a commercially available CFD code can successfully predict vortices, and these models have not been used extensively in design of basins with pump intakes.

1.2 Objective and Scope

The objective of this thesis is to determine whether CFD can be used to predict the occurrence of vortices in the vicinity of pump intakes. A series of numerical simulations is compared with experimental observations to quantitatively define the applicability of CFD for these problems. For the purpose of this thesis, the goal is to address the practical application of CFD in current design practices, therefore, a commercially available CFD software package was used for the comparison. Furthermore, due to the difficulty in modeling circulation in swirling flows, the scope of this thesis emphasizes the use of CFD to predict the occurrence of vortices and swirl rather than the use of CFD to predict the velocity distributions within swirling flows. This information will provide a basis for a longer-term

objective of applying CFD as a design tool for investigating alternative measures necessary to ensure effective design and operation of pump intakes.

1.3 Methodology

The methodology includes experiments completed in a physical model along a series of numerical simulations using a package CFD code. First, physical experiments were set up and completed using a simple pump intake model constructed at Alden Research Laboratory, Inc. (ARL) in Holden, MA. This model was used in previous hydraulic model studies and was reconstructed for this project. A series of test were completed to ensure the apparatus could provide experimental conditions that represented flow approaching a typical pump intake. Experiments were completed using this simple pump intake model under various flowrates to define a set of flow conditions with varying degrees of vortex development. Next, the series of simulations was completed using FIDAP, a commercial CFD software package, to characterize the flow in the vicinity of a pump intake. The numerical model configuration was developed to simulate the actual conditions in the physical experimental setup. The approach for the numerical modeling involved the initial use of the parameters used in the physical experimental model, and direct comparison between experimental results and model predictions. It also included subsequent sensitivity analyses to address the sensitivity of the model predictions to the inherent assumptions and associated parameters.

1.4 Outline

After a brief summary of background literature in Chapter 2 (which describes some of the processes affecting pump intake vortices as well as the parameters used to describe them), Chapter 3 describes the experimental setup and conditions. Chapter 4 contains results pertaining to observations and measurements of the vortices observed in the pump intake model. These observations are used to establish a base case model for numerical

simulation. The development of the base case numerical model is subsequently presented in Chapter 5, followed by a comparison of the model predictions with experimental results. Chapter 5 also describes a set of simulations to assess the significance of some model assumptions and parameters. Finally, Chapter 6 concludes with a review of the implications of the results in this thesis in regards to the long-term objectives.

2.0 Background

Many investigations have been performed that address the nature of vortices. These studies include such subjects as what causes vortices to form, how to prevent them from forming, and how to predict the formation of vortices. These studies have led to better understanding of the science of vortices. This background section provides a discussion of mechanisms in vortex formation, free surface and air water interfaces, design criteria, vortex classifications, and previous investigations into the use of computational fluid dynamics (CFD) models in vortex predictions.

2.1 Mechanisms Involved in Vortex Formation

A number of focused experimental and numerical investigations have provided insight into the fundamental processes leading to the development of vortices at inlets such as pump intakes. For example, Shin et al. (1986) demonstrated that two basic mechanisms lead to inlet vortex formation. The first mechanism involves the development of an inlet vortex due to the amplification of ambient vorticity in the approach flow as vortex lines are convected into the inlet. The second mechanism involves the development of a trailing vortex in the vicinity of the intake as a result of the variation in circulation along the inlet. For this second case, a vortex can develop in a flow that is irrotational upstream, and the vortex development therefore does not depend on the presence of ambient vorticity. The investigations on kinematic parameters, completed as part of Shin's investigation, indicate that the strength of an inlet-vortex/trailing vortex system increases with decreasing distance from the surface. However, for an inlet in an upstream irrotational flow, two counter-rotating vortices can still trail from the rear of the inlet. Causes of vortex motion, however, are still difficult to define for most practical situations.

2.2 Free Surface and Air Water Interface

Vortices in the vicinity of pump intakes may be adjacent to the channel bottom or a channel wall (i.e. submerged vortices) or they may appear adjacent to the free surface (i.e. free surface vortex). By studying the way that the way that vorticities interact with the free surface, more information can be known about the characteristics in vortex formation and possibly better prediction methods can be developed as a result of such studies.

The study of vorticity interactions with the free surface requires consideration of the dynamics of a vorticity field bounded by a deformable surface. The surface deforms to satisfy the conditions that the tangential stress is equal to zero and the normal stress is equal to a constant at all times. According to Rood (1995), the interaction between vorticity and the surface is characterized by both the vorticity and flux of the vorticity at the free surface, the deformation of the free surface, and the dynamic behavior of the velocity field. The stresses at the interface between the two fluids (air and water) must be in balance, such that:

$$(\text{stress})_{\text{water side of interface}} + (\text{stress})_{\text{air side}} + (\text{stress})_{\text{surface}} = 0 \qquad (2\text{-}2)$$

When describing the local details of flow at the free surface, viscous forces normally cannot be neglected, especially when describing the vorticity generated by the deformation. However, when localized flow details are not of concern, there are instances when the viscous terms can be neglected. By neglecting viscous forces, and order of magnitude estimate of the deformations can be obtained. For estimates of free surface deformation, the approximation is appropriate when the viscous force is much less than the inertial force. This condition typically occurs when the flow is at a high Reynolds number.

The conditions under which viscous terms can be neglected in estimates of free surface deformation arise for two different classes of vorticity distribution. Motions of flow in the first class are unsteady and irrotational. They are defined with vortices and feature values for vorticity that are practically equal to zero at locations away from the

relatively small viscous core. Here, it can also be assumed that there are no viscous forces affecting the evolution of the flow near the free surface. Flows in this class can be considered irrotational in the domain excluding the core and particularly near the free surface.

Motions for flows in the second class are quasi-steady and rotational. They are characterized by vorticity that has diffused so that the "core" is extensive in area. Although the vorticity associated with these motions is nonzero and the flow rotational, the viscous forces have a long time scale relative to the faster time scale for the flow inertia.

For both of the above classifications of vortex motion, the momentum equation can be integrated along a streamline and, in particular, along the free surface to arrive at estimates for the deformation. The procedure uses the Bernoulli equation to provide estimates of the surface deformations associated with vortex interactions, which leads to the following equations.

$$\partial u/\partial t + \nabla(u^2/2 + p/\rho + gz) = \nabla H_s \tag{2-3}$$

$$\nabla H_s = \mathbf{u} \times \omega \tag{2-4}$$

where ω is the vorticity, u is the velocity, p is the pressure, ρ is the density, g is the gravitational acceleration, z is the depth, and H_s is a constant on the free surface. Deformed or curved free surfaces are generally accompanied by vorticity even if the bulk interior flow flows contain no vorticity.

The development of the vorticity boundary condition at a free surface follows several steps. These steps effectively combine the requirements for surface curvature and zero tangential stress on the interface to specify a nonzero value for the surface parallel component of vorticity at the free surface. This nonzero surface vorticity can exist even when potential flow exists in the interior of the fluid.

Rood (1995) defines the free surface in the cylindrical polar coordinate system so that the free surface is coincident at some instant with the surface. The equation for the vorticity parallel to the free surface, along the z-axis, is:

$$\omega_s \quad \frac{\partial u_\theta}{\partial r} \quad \frac{u_\theta}{R} \quad \frac{}{R}\frac{\partial u_r}{\partial \theta} \tag{2-5}$$

where ω_σ is the vorticity at the surface, u_θ is the normal velocity, u_r is the radial velocity, r is the radial position, R is the radius, and θ is the radial distance. The first and second terms on the right side of the equation are the contributions provided by the spatial change in the velocity. The third term, if nonzero, implies a velocity of the free surface normal to itself. The second term is peculiar to curved surfaces, and states that a surface-parallel component of velocity contributes to the vorticity. For flat surfaces the second term disappears, but the third term does not. (Rood 1995) These considerations can help to define a boundary condition for vorticity at the free surface.

Even though the interactions of the air water interface can have implications related to the nature of free surface vortices, many investigations believe that they are not critical factors in the occurrence of vortices adjacent to a pump intake. Consequently, many investigations do not account for the presence of the free surface. Rather, these investigations will assume that the free surface is a fixed boundary (or wall). In this case, the vortex development is primarily driven by the mechanisms discussed in Section 2.1. Similarly for the purpose of this thesis, the role of the free surface also is not explicitly considered in vortex development. Accordingly, this thesis concentrates on practical design applications such as the use of a fixed top boundary and the effects of the free surface are left for future work.

2.3 Design Criteria

A number of guidelines have been developed for the design of pump intakes. The most widely used design guidelines are those published by the British Hydrodynamics Research Association, the Hydraulic Institute Standards (1975), and the US Army Corps of Engineers. These guidelines provide recommendations on the size and configuration of pump sumps based on either the suction bell diameter or the anticipated flow rates. However, none of these guidelines guarantee satisfactory flow conditions and all of the guidelines point out that favorable approach flow conditions are necessary. Unfortunately, from experience, it is known that relatively small geometric details just upstream of the pumps, or any flow conditions that are less than optimal, can have an effect on flow patterns entering a pump and on pump performance. An unsatisfactory approach flow distribution can produce eddies and pre-rotation of the flow entering the pump (as indicated by a flow swirl angle greater than 5°).

Strong surface eddies can form vortices ranging from dye core vortices to full air cores, and rotation near the pump bell can form submerged vortices which, although not visible to the eye can have significant consequences. These disturbances cause extensive pump vibration, noise, cavitation, and a reduction in flow capacity. In extreme cases, pump columns and bells have separated, and drive shafts of wet pit pumps have broken.

According to Sweeney (1982) the following are possible flow conditions that can result in problems in pump performance.

1. surface vortices may draw air from the free surface into the pump, causing unbalanced loading of the impeller, periodic vibration, and reduction in pump capacity
2. subsurface vortices which may emanate from the floor, side or back walls, or both, and in the case of pressurized wet-pit sump, from the ceiling, entering the pump and causing vibration and cavitation

3. prerotation of flow entering the pump, which will change the angle of attack of the impeller blades from the design value and may affect pump efficiency and cause cavitation
4. an uneven distribution of flow at the pump throat which may results in unbalanced loading of the impeller
5. significant time fluctuations in velocities at the pump throat, which may cause vibration and cavitation
6. separation of flow from the pump suction bell surface extending to the throat, a problem of pump rather than sump design, which may cause a nonuniform flow field at the impeller and possible cavitation

Also according to Sweeney (1982), some hydraulic conditions that can cause pump problems and deficiencies include:

1. uneven flow distribution in the sump causing a net flow circulation around the pump column
2. large-scale turbulence generated in the approach to the sump
3. vorticity generated by flow past pier noses, screen supports, and other structural members
4. vorticity generated at fluid shear zones formed at discontinuous flow boundaries in the vicinity of the pump
5. vorticity generated in the boundary layer at the sump walls and floor
6. vorticity generated by flow past the pump column
7. air-entrainment

While the causes of pump problems and deficiencies caused by flow conditions in the sump have been well established, but their solutions have not.

2.4 Vortex Classifications and Scale Effects

Another problem influencing the reliability of vortex severity predicted by hydraulic models for decades is scale effects. The fluid phenomena involved are such that vortices would be less severe in a model than in the actual (prototype) installation. The concern is that prototype conditions could be considerably worse than predicted with consequential undesirable results for the project operation.

To aid in estimating the significance of vortex problems, Hecker (1984) proposed a scale to classify vortex strength using the vortex classification types listed in Table 2-1. Figure 2-1 depicts examples of each vortex type. Vortices can be classified according to their strength ranging from a Type 1 vortex, which is described as an incoherent surface swirl, to a Type 6 vortex, which is a full air core extending to the intake.

Hecker (1984) also pointed out that the vortex type is a function of five parameters:

1. a relative submergence (h_∞/d),
2. a circulation number $\Gamma_N = \Gamma\rho_o/Q$,
3. a Froude number $F_N=[Q/dh_\infty)]/\sqrt{gh_\infty}$,
4. a Reynolds number $Re = Q/(\nu h_\infty)$, and
5. a Weber number $W_N = [Q/(dh_\infty)]^2/[\sigma/\rho_o d)]$.

Variables in these parameters include the discharge (Q), the fluid density (ρ_o), the diameter of the pump intake (d), the water depth of the approach flow (h_∞), the surface tension (σ), the circulation (Γ), and the kinematic viscosity (ν).

Table 2-1: (Hecker 1984)

Vortex Classifications	
1	incoherent surface swirl
2	surface dimple; coherent swirl at surface
3	dye core at intake; coherent swirl throughout water column
4	vortex pulling floating trash, but not air
5	vortex pulling air bubbles to intake
6	full air core to intake

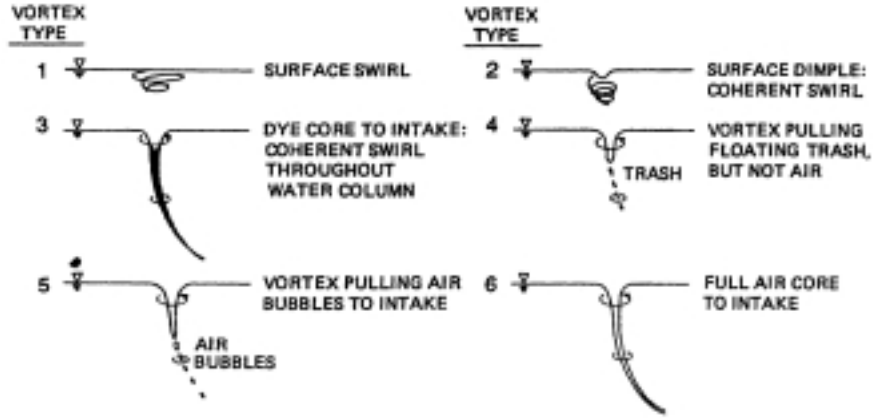

Figure 2-1: Vortex Classifications (Hecker 1984)

One possible difficulty in scale modeling is that it is impossible to reduce all pertinent forces by the same factor. With Froude-scale models, the inertial and gravitational forces are reduced similarly, but the viscous and surface tension forces cannot be simultaneously reduced. The extra influence of these forces is known as a “scale effect”. For pump intake models, these scale effects become increasingly important with increasing vortex type. A number of investigations (e.g. Padmanabhan and Hecker, 1984) have indicated that the scale effects for the model are avoided if the Reynolds number, based on the inlet flow and submergence or intake diameter, exceeds approximately 3×10^4, and the Weber number exceeds 150. At Reynolds numbers higher than 3×10^4 viscous scale effects are considered negligible.

Another parameter, the swirl angle (θ), is defined by Hattersely (1985) as:

$$\theta = \tan^{-1} \frac{\pi n d}{U_p} \tag{2-1}$$

where U_p is the axial velocity in the pump intake at the swirl meter location, d is the intake diameter, and n is the rotation rate of the swirl meter in revolutions/second. Adequate design typically requires the vortex classification to by less than Type 3 and θ to be less than 5°. Since these parameters are commonly used in practice, they provide an appropriate basis for qualifying the conditions and observations associated with numerical and experimental results in the present investigation.

2.5 CFD Models

CFD has not been used extensively to model pump intake hydrodynamics. However, some recent research has been completed at the University of Iowa, which has provided some insight into this application of CFD. Constantinescu and Patel (1997) summarized the development of a computational fluid dynamics (CFD) model, and investigated the application of various turbulence models (κ–ε and low and high Reynolds number κ–ω models) in predicting vortices at an asymmetrically-located pump intake. This investigation revealed that the locations and shape of predicted vortices varied slightly depending on the turbulence model selected. Consequently, the authors recommended a two-layer model to resolve finer aspects of the vortices. That analysis also provided the basis for a more detailed description presented in Constantinescu and Patel (1998), in which the authors described the numerical model in detail, and applied this model to the geometry and conditions associated with a 1.2-m long by 0.52-m wide by 0.55-m deep pump intake model. The results presented in this thesis complement the efforts of Constantinescu and Patel by applying an established commercially available software package.

3.0 Experimental Setup and Methodology

In order to assess the applicability of Computational Fluid Dynamics (CFD), it is necessary to have some experimental data which can be used to validate the CFD predictions. Experimental studies on the formation of vortices in a simple pump intake model were conducted at Alden Research Laboratory, Inc. (ARL) in Holden, MA. The experimental setup and procedures are presented below in this chapter.

3.1 Experimental Setup and Flow Conditions

The experimental setup consists of a pump intake model, which was provided by Alden Research Laboratories, Inc (ARL). Plan and profile views of the model are shown in Figures 3-1 and 3-2. The model consists of a 3.18-m long, 0.56-m wide flume with a 13.34-cm diameter pump intake on one end and an inlet on the other end. The geometry of the channel was designed in accordance with standards recommended by the Hydraulic Institute Standards (Hydraulic Institute 1975). Water is recirculated from the pump intake to the inlet through a centrifugal pump and 0.21-m PVC piping that accommodates steady flowrates ranging from 0 to 0.03 m^3/s. Photographs of the tank and the piping are shown in Figure 3-3 and 3-4. The intake and pump are shown in Figure 3-3 and the inlet with some of the filter material is shown in Figure 3-4. The piping rises from the intake up to a height of approximately 1.67-m, the piping then extends to the floor and extends to the other side of the tank, where it then rises to the top of the tank and enters the tank. The flow of the tank is regulated with a butterfly valve and a venturi meter is used to monitor the flow rate. The startup procedures for the operation of the model are included as Appendix A. Additional photographs of the experimental setup are included in Appendix B.

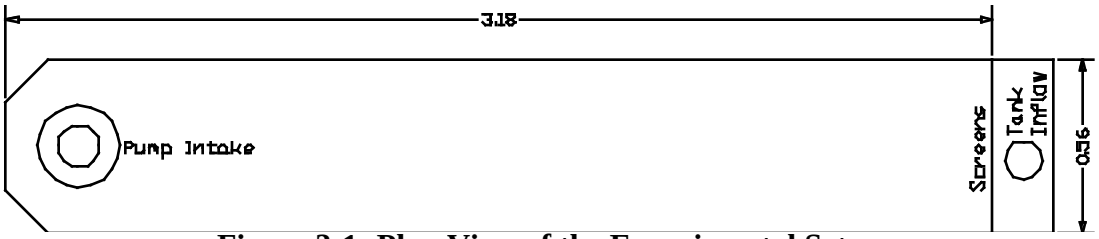

Figure 3-1: Plan View of the Experimental Setup

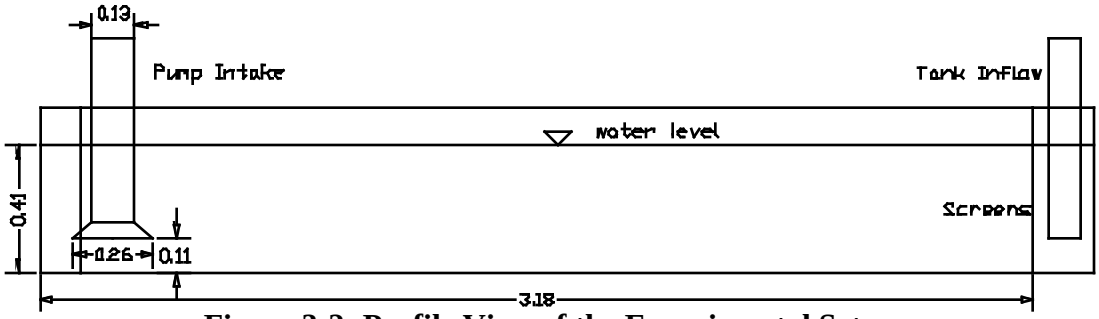

Figure 3-2: Profile View of the Experimental Setup

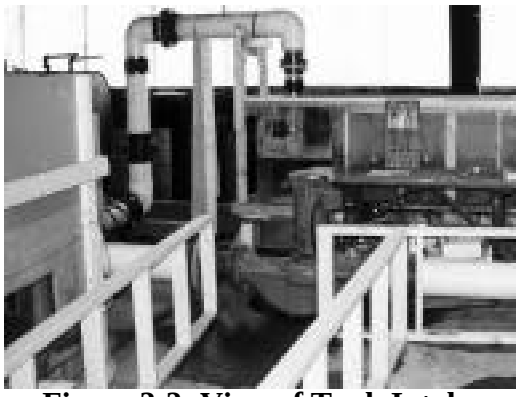

Figure 3-3: View of Tank Intake

Figure 3-4: View of Tank Inlet

For the purpose of this study, the distance between the pump intake and the bottom is set within design standards and this variable's effect on vortex formation is not considered further. Similarly, while it is well known that the depth of submergence of a pump intake will affect the development of vortices and swirl, the scope of this study only considers the development of vortices in a single water depth for which vortices will occur for sufficiently high flowrates. Here, the depth is selected to be 0.41 m, which matches the depth used in previous model studies completed using the same physical model.

3.2 Velocity Measurements

Velocities were measured using a Sontek Acoustic Doppler Velocity (ADV) probe. The Sontek ADV probe is comprised of an acoustic sensor. The sensor is an assembly of three acoustic receivers and one acoustic transmitter, mounted on a 40-cm stainless steel stem. The configuration provides velocity measurements over a sampling volume of approximately 0.3 cm^3, which effectively yields point velocity measurements with three-components (in x, y, and z). The velocity probe uses a data acquisition interface to convert the data points into velocity measurement. In order to confirm velocity measurements, pitot tubes and pressure gauges were also set up to take confirmatory velocity readings. However, due to equipment and time restraints, the pitot tubes were not used. For the purposes of this thesis, the velocity measurements were used to provide information on the mean velocity only.

Cross sectional velocity distributions were obtained by defining a grid over the cross section of the tank. The velocity was measured with the ADV probe in the center of each grid block. Figure 3-5 shows a sample of the sampling locations. For this case the area was divided into 9 sections each measuring 13.55-cm high by 18.63-cm wide. The samples were then taken in the center of each block. For example, sample 6 was taken at height of 20.3 cm from the tank bottom and 46.6 cm from the left side of the tank (as viewed looking downstream towards the pump intake).

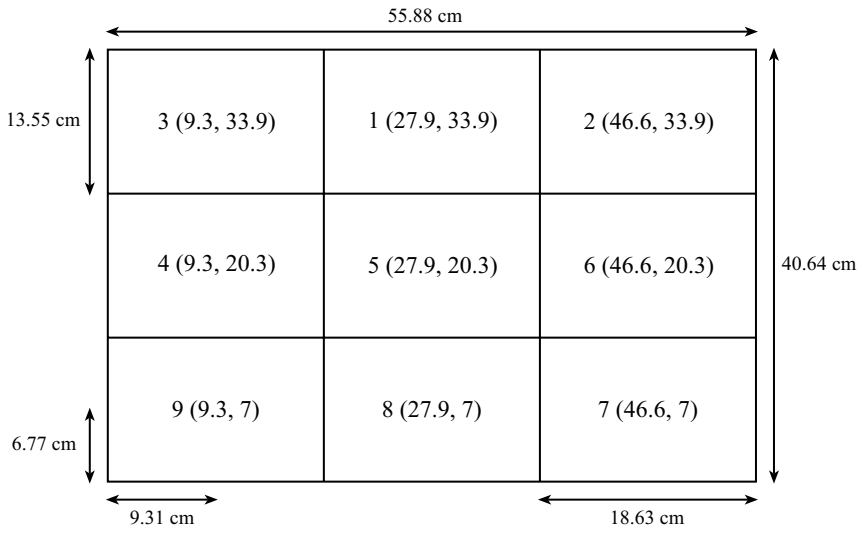

Figure 3-5: Sample Locations Taken 30 cm From the Screen for Q = 0.0197 m^3/s

3.3 Flow Measurements

A venturi meter and a manometer board were used to measure the flow in the tank. The taps to the manometer board were connected to the venturi meter at the narrowest part of the meter and at the widest part of the meter. By measuring the differences in pressure in these two parts of the meter the flow rate can be determined. The readings were taken by measuring the differences in heights in the manometer tubes and by using the following formula:

$$Q = 0.7249 * \sqrt{\Delta h} \tag{3-1}$$

where, Δh is the difference in height in feet and Q is the flowrate in ft^3/s. This equation was developed by ARL staff specifically for this venturi meter. The flow readings were checked before, during, and after all samples were taken to ensure that the flow did not fluctuate during the sampling.

3.4 Required sampling time

Since the flow in the tank is extremely turbulent, it is necessary to determine a required sampling duration to ensure that mean velocities will be appropriate. Required sampling time was determined by taking repeated velocity records at selected locations. Then, the average velocity and standard deviations were calculated for various time intervals. The average velocity was calculated for the time intervals that were successively increased by 2 minute durations to cover a range of durations between 2 to 20 minutes (i.e. 0 to 2 minutes, 0 to 4 minutes, 0 to 6 minutes …0 to 20 minutes). A similar procedure was used to determine standard deviations for various time intervals. The velocities and standard deviations were then plotted and a sufficient sampling time was determined. As seen in Figure 3-6 and 3-7, the average velocity and standard deviation became uniform at approximately 12 minutes. Based on this information, a sampling time of 15 minutes was

chosen to be conservative. The velocities shown in these figures were taken 30 cm from the inlet screen at a height of 20.32 cm from the bottom of the tank and 9.31 cm from the left side of the tank (as viewed looking downstream towards the intake).

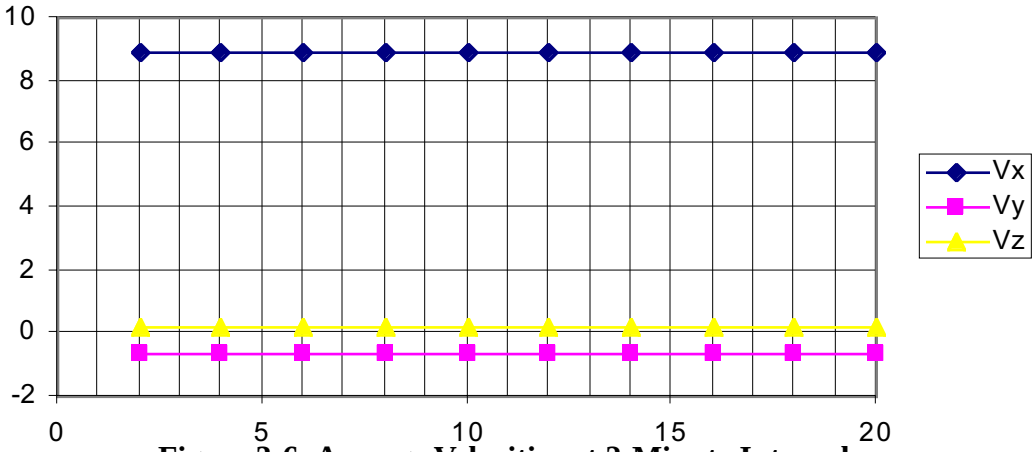

Figure 3-6: Average Velocities at 2-Minute Intervals

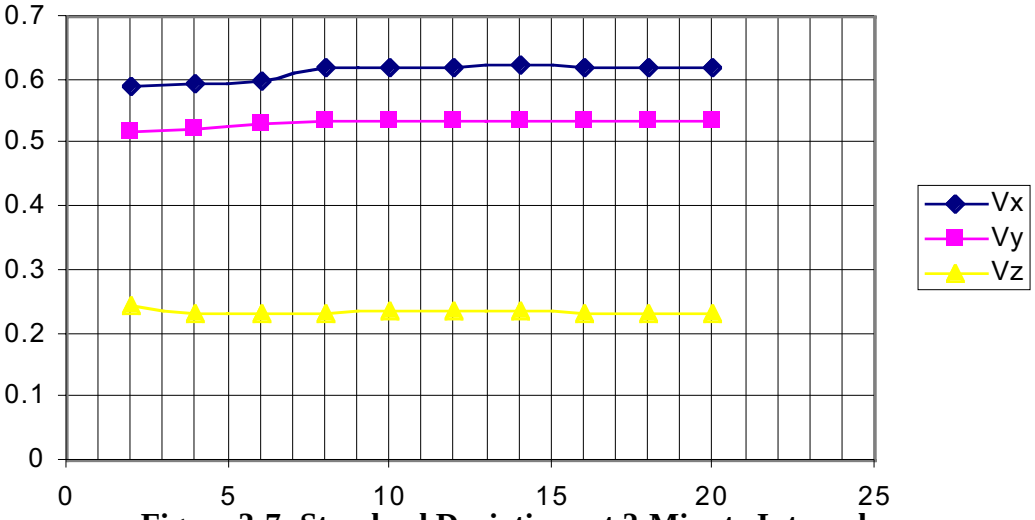

Figure 3-7: Standard Deviations at 2-Minute Intervals

3.5 Cross-sectional Flow Distributions

3.5.1 Inlet Velocity Profile

A cross-sectional velocity profile was taken immediately downstream of the inlet (30-cm from the screen) to verify that the velocity of the flow entering the test section of the tank was uniform over the cross-section. These velocity measurements were used to de-

velop a filter system consisting of a series of screens and filter material, which was located immediately downstream of the inlet to straighten the flow and ensure a uniform velocity distribution exists at the inlet. Figure 3-8 shows the velocity distribution at the inlet for a flowrate of 0.0197 m^3/s. This figure shows that the velocity is higher near the top of the sampling area. However, the flow is fairly uniform and for the purposes of this thesis, this is an acceptable velocity distribution.

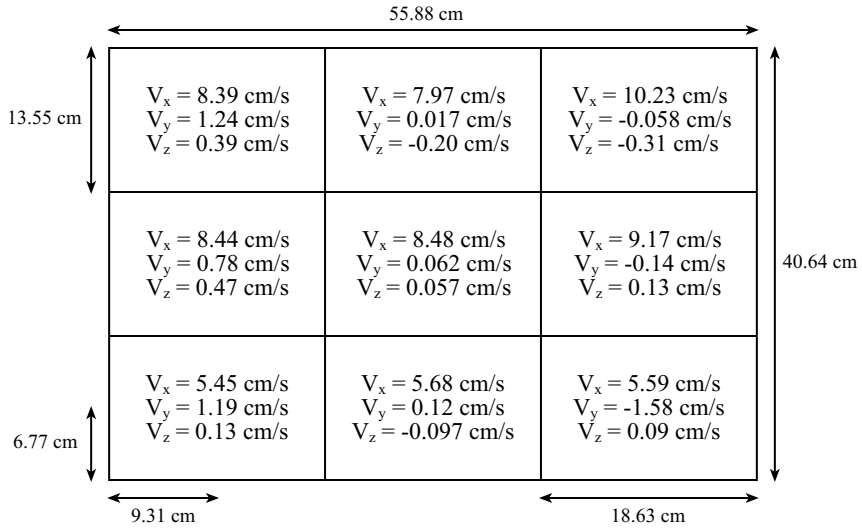

Figure 3-8: Velocity Distribution Near the Inlet Taken 30 cm From the Screen For Q = 0.0197 m^3/s

3.5.2 Additional Measurements

Additional velocity profiles were measured immediately upstream of the pump intake and dye was also injected in numerous locations to gain a better understanding of the flow field approaching the pump intake. A swirl meter was located in the intake pipe, which provided information on the characteristics of the flow within the pump intake. The swirl rate in the intake was determined by counting the rotations of the meter. The swirl measurements, the ADV measurements, and the observations made with the dye injections will be discussed in the following section.

4.0 Physical Experiments

Once the tank and sampling equipment were set up, the next step was to conduct the physical experiments. The purpose of the physical experiments was to observe the qualitative aspects of the vortex development. In order to do this three cases were used. The first case had a flowrate of 0.0197 m^3/s and an average velocity of 8.65 cm/s. Because clearly defined vortices were observed with minimal free surface undulations for this flow condition, this case was selected as a base case simulation for both the physical experiments and the numerical model development. The second case used was one with a higher flowrate of 0.0237 m^3/s and the third case was one with a lower flowrate of 0.0133 m^3/s. A more detailed discussion of the cases and why they were chosen is included below.

4.1 Base Case

For the first setup for the model, a flow rate of 0.0197 m^3/s was chosen. This condition was selected because it has a high Reynolds number of 3.6×10^4 and consistently formed clearly-defined Type 2 and 3 vortices near the intake. Since this case provided an effective basis for comparison (due to its clearly defined vortices), this case is defined as the "base case" throughout the remainder of this thesis.

4.1.1 Visual Observations

For the base case flow rate, visual observations revealed that the vortices formed to the right and behind the pump intake and travel further to the right of the intake as illustrated in Figure 4-1. After reaching the right of the tank, the vortices dissipated and then started reforming again behind the intake. The initial location of the vortex is shown by the "o" and the line illustrates the typical path of the vortex. For the base case of 0.0197 m^3/s dimples were seen forming and occasionally debris would be dragged into the vortices. Type 2 vortices (surface swirls) consistently were observed without the addition of dye. As noted above, the vortices that formed with this flow condition ranged from a surface swirl

(vortex type 2) to a dye core (vortex type 3). The swirl motion also affected flow within the pump intake. Swirl measurements were obtained by observing the rotation of the swirl meter located inside the pump intake. The swirl present in this condition was 52 rev/min with a swirl angle of 14.5^{o}, as measured by the swirl meter.

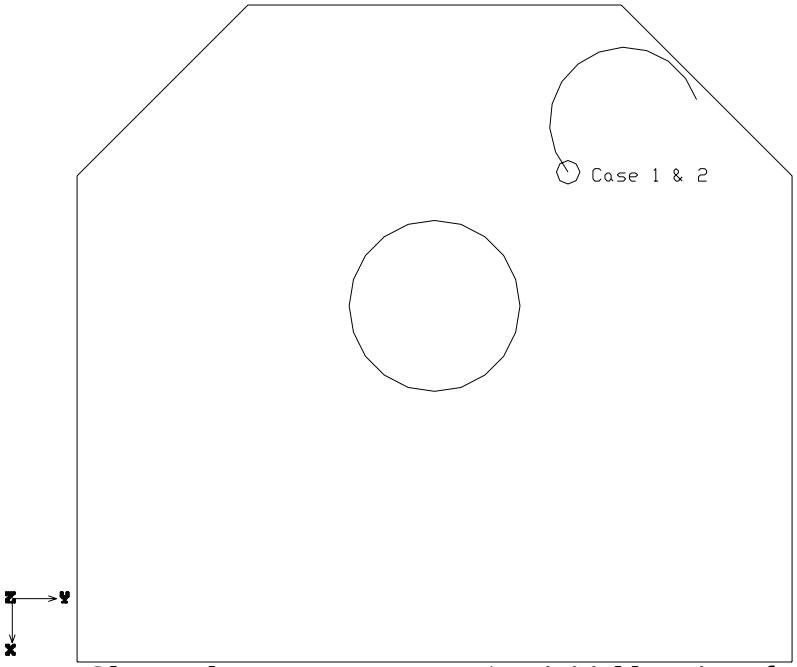

Figure 4-1: Observed vortex movements (o = initial location of vortex)
Case 1: Base Case, Case 2: High Reynolds Number (Re = 4.2x10^{4})

4.1.2 Velocity Measurements at the Tank Inlet

Velocity measurements were taken at the tank inlet, at a location 30 cm from the inlet screens, to ensure that the flow entering the tank was uniform over the cross section. Figure 3-8, located in the previous chapter, shows the velocity distribution for the base case flowrate of 0.0197 m^{3}/s. This figure shows that the velocity is higher near the top and left of the sampling area. However, as discussed previously, this distribution was considered to be sufficient for the purpose of this thesis.

4.1.3 Velocity Measurements Near Pump Intake

The flow conditions present in the tank were defined by taking measurements of the velocity at a location 25 cm upstream of the pump intake for all flow conditions. This approach helped to show the formation of boundary layers near the bottom of the tank and the flow characteristics near the intake. For these experiments the velocity distribution was obtained using a more detailed grid than that shown in Figure 3-5. The measurement locations for this grid, which included 16 locations, are shown in Figure 4-2. The velocity distribution near the intake for the flow rate of 0.0197 m^3/s, as viewed looking downstream towards the intake, is shown in Figure 4-3. Figure 4-3 lists the x, y, and z components of the velocity (V_x, V_y, and V_z), respectively at different locations over the cross-section. The figure illustrates that the velocity distribution is fairly uniform. The highest velocities in x (V_x) are located near the water surface. High V_x values also exist at the bottom of the tank due to the intake of the model drawing the flow towards it. However, the velocities in y (V_y) are all slightly positive, indicating a net movement of flow towards the right of the tank. Also high velocities in x (V_x) exist near the surface to the left of the pump intake. The velocities in z are all directed downward towards the pump intake. It is likely that the presence of these flow patterns has some role in causing the vortices to form to the right of the intake and then drift toward the wall to the right of the intake.

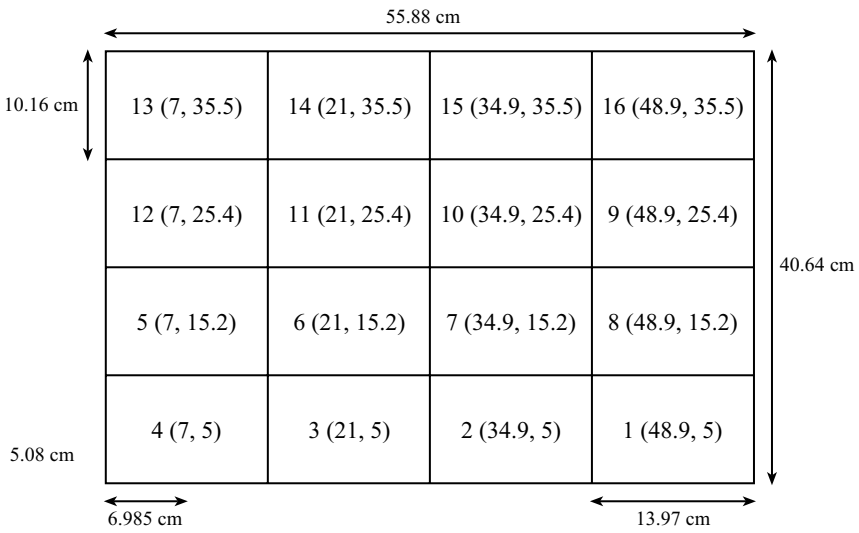

Figure 4-2: Sample Locations

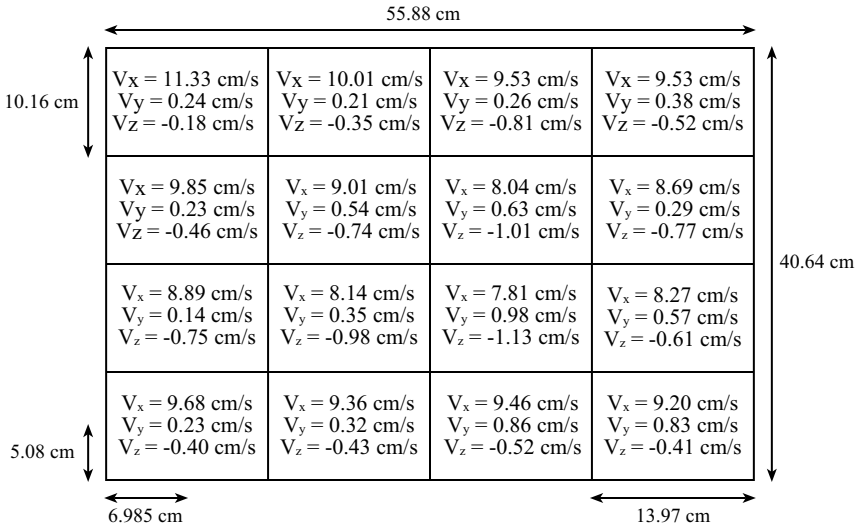

Figure 4-3: Velocity Distribution Near the Intake For Re = 3.6×10^4

4.1.4 Visual Observations with Dye

Unless the vortices that are forming are Type 5 or 6 vortices and are pulling air bubbles into the water or forming full air cores, they cannot be properly classified without help. Therefore, dye must be injected into the subsurface to fully understand the characteristics of the vortices that are present. Without the aid of dye, all that can be observed are surface swirls and dimples. To observe the vortices the dye was injected directly into the vortex. With the addition of dye, dye core vortices (Type 3) could be observed forming behind and to the right of the intake. Thus, the dye test verified that the dye core vortices extended from the surface down to the intake. The dye was also injected into the subsurface at several locations. Regardless of the depth, the dye was drawn directly into the pump intake. Consequently, while the surface dye core vortices were evident, no additional vortices existed.

4.2 High Reynolds Number

For the second case for the model, a higher flow condition of 0.0237 m^3/s was chosen. This condition was selected since it has a high Reynolds number of 4.2×10^4 and vortices consistently formed for this flow condition. The purpose of this case was to assess

the motion of the vortices at extremely high Reynolds number, and compare the circulation patterns with those of the base case.

4.2.1 Visual Observations

For this second case, the vortices would again form to the right of the intake and then proceed to the right of the intake. However, these vortices were stronger and typically ranged from dye core to vortices pulling air bubbles into the intake (vortex type 3 to 5). The typical path of the vortices that formed in this flow condition followed the same trajectory as that for the base case. Therefore, its trajectory is the same as that illustrated in Figure 4-1. The swirl in this condition increase from 52 rev/min (for the base case) to 60 rev/min and the swirl angle increased to 13.9°.

4.2.2 Velocity Distribution at the Tank Inlet

A velocity profile was taken near the inlet at a location 30 cm from the screens. The locations of the samples are shown in Figure 4-2. The velocity profile is depicted in Figure 4-4. The profile is similar to the profile that was present in the base case. Again, flow is highest near the top of the sampling area.

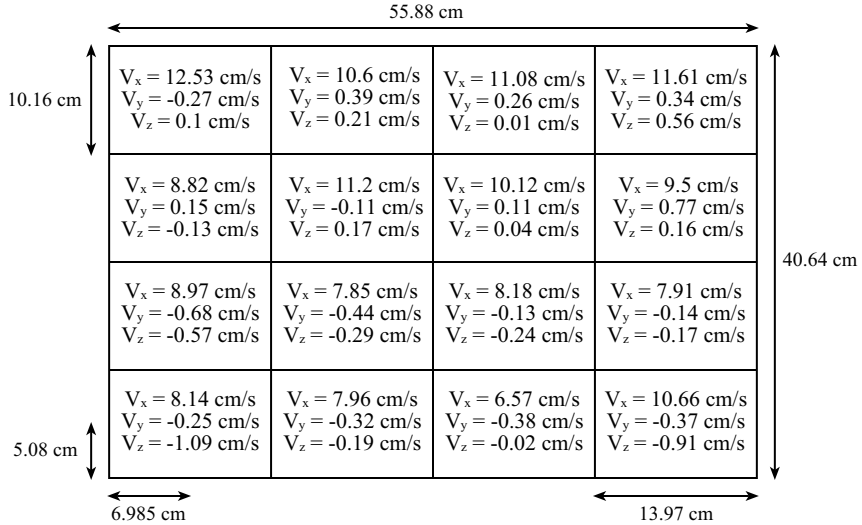

Figure 4-4: Velocity Distribution Near the Inlet For Re = 4.2×10^4

4.2.3 Velocity Distribution Near the Pump Intake

Velocity measurements near the pump intake were taken at the same location as the measurements for the base case and are shown in Figure 4-5. The velocity distribution for this case is similar to the distribution that was present in the base case. Flow is highest in x (V_x) near the water surface and to the left of the pump intake. As in the base case, the velocities in y (V_y) are all slightly positive, indicating a net movement of flow towards the right of the tank. The velocities in z (V_z) are all directed downward towards the pump intake. As before, it is likely that these flow patterns are the cause of the vortices forming to the right of the intake and continuing to rotate towards the right of the intake.

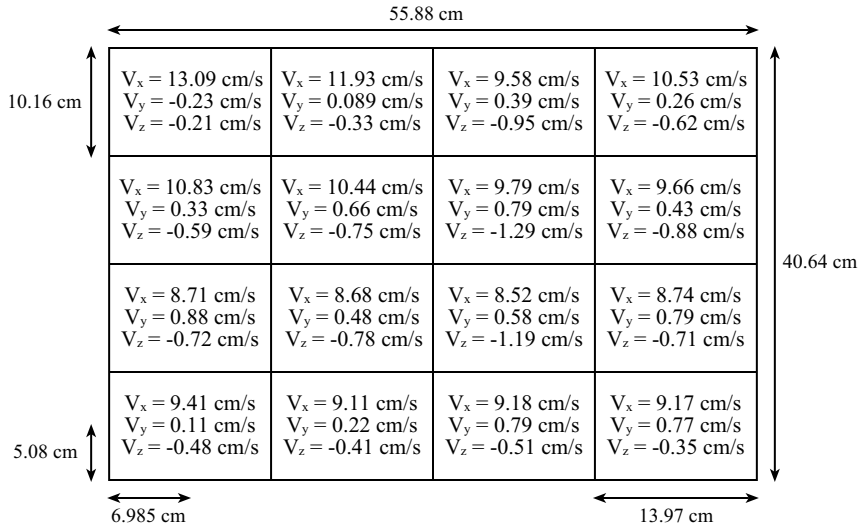

Figure 4-5: Velocity Distribution Near the Intake For Re = 4.2×10^4

4.2.4 Visual Observations with Dye

When dye was injected into the subsurface at several locations, the dye always flowed directly towards the intake, with no evidence of swirl present in the tank. When dye was injected directly into the surface swirls that were present, dye cores could be observed consistently forming behind and to the right of the intake. In this case, Type 5 vortices could occasionally be observed pulling air bubbles into the intake.

4.3 Low Reynolds Number

The third case observed was of a lower flow condition. Here, the flow rate used was 0.0133 m^3/s, which results in a Reynolds number of 2.4×10^4. This flow condition was selected since its Reynolds number is well below the value of 4×10^4, which Hecker (1984) recommends as a minimum to avoid scale effects.

4.3.1 Visual Observations

For this third case, visual observations revealed that Type 1 vortices consistently formed. The vortices would form directly behind the intake and would again travel to the right of the intake before dissipating. However, the typical paths of the vortices that formed under this flow condition were different than the paths of the vortices that typically formed under the base case and high Reynolds number conditions. The typical path of the vortices of this case in comparison to those of the base case and high flow conditions is shown in Figure 4-6. The swirl and the swirl angle were 38 rev/min and 11.7°, respectively.

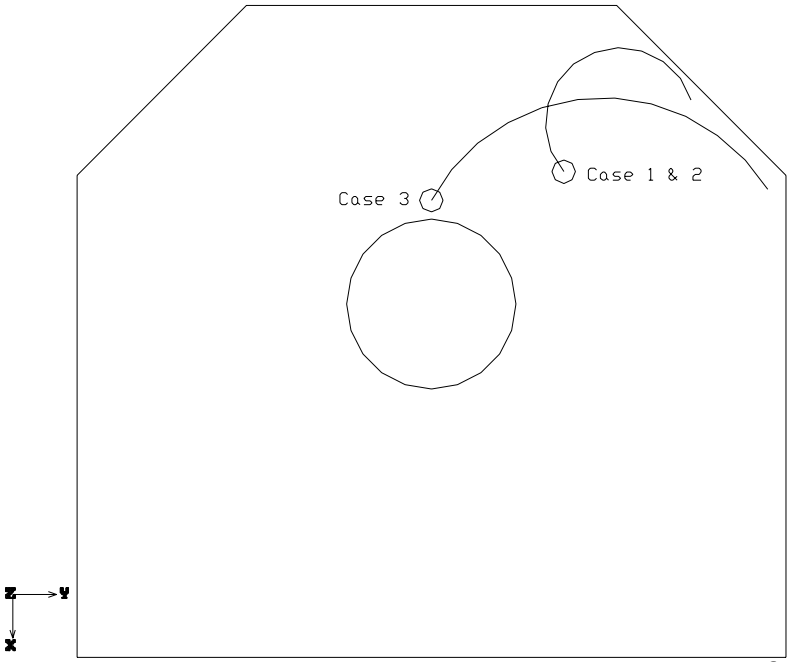

Figure 4-6: Observed vortex movements (o = initial location of vortex)
Case 1: Base Case, Case 2: High Reynolds Number ($Re = 4.2 \times 10^4$)
Case 3: Low Reynolds Number ($Re = 2.4 \times 10^4$)

4.3.2 Velocity Measurements at the Tank Inlet

As in the previous cases, a velocity profile was taken near the inlet of the tank at a location 30 cm downstream of the screens. The sample locations were the same as those in the high flow condition. Figure 4-7 shows the velocities in the x, y, and z directions for this flow rate. Flow patterns that were observed in this case were similar to both the base case and the high flow case. The velocities were again highest near the top of the sampling area.

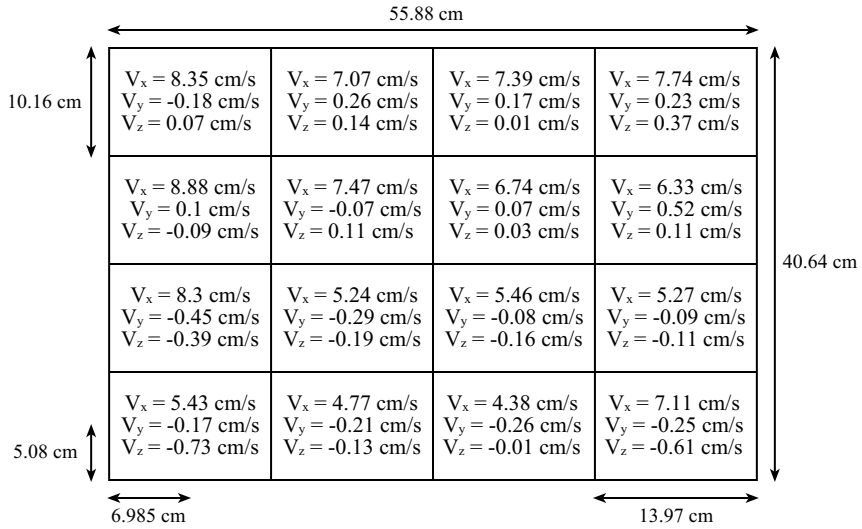

Figure 4-7: Velocity Distribution Near the Inlet For Re = 2.4×10^4

4.3.3 Velocity Measurements Near Pump Intake

The velocity measurements near the pump intake were taken at the same location as the measurements for the base case and are shown in Figure 4-8. The velocity distribution for this case is similar to the distributions that were present in both the base case and the high flow case. Flow was highest in x (V_x) to the left of the pump intake near the water surface. As in the previous cases, the velocities in y (V_y) are all slightly positive, indicating a net movement of flow towards the right of the tank. The velocities in z (V_z) are all directed downward towards the pump intake and continuing towards the right of the intake.

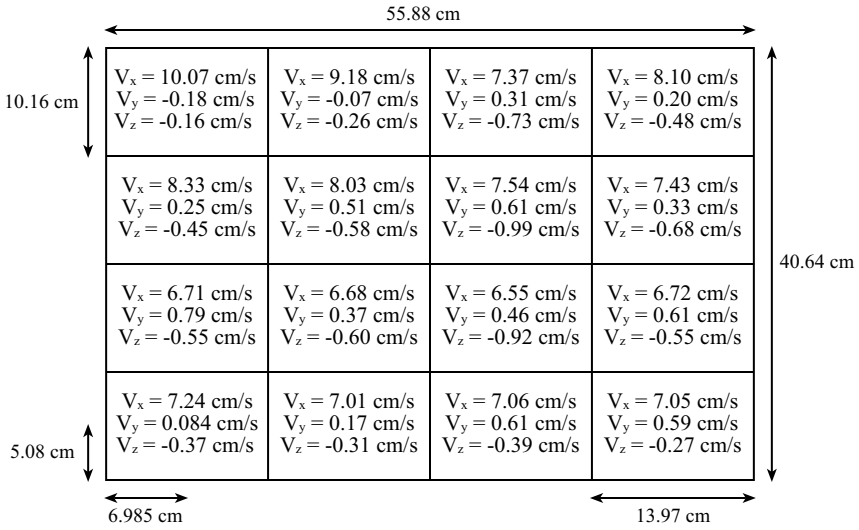

Figure 4-8: Velocity Distribution Near the Intake For Re = 2.4×10^4

4.3.4 Visual Observation with Dye

For this flow condition, surface simples and swirls could be observed behind and to the right of the intake. Since the vortices in this case were primarily at the surface, the addition of dye did not reveal significant dye core vortices forming under this flow condition. As in the two previous cases, when dye was injected into the subsurface at various locations, it was immediately drawn towards and into the intake indicating that there was no subsurface swirl present.

4.4 Summary

The characteristics of the flow, vortex formations, and the swirl for these three cases are summarized in Table 4-1. Dye injections revealed no wall-attached subsurface vortices for any of the three cases. However, for all three cases swirl was observed in the pump intake and free surface vortices were observed in the vicinity of the pump intake. The vortices in Table 4-1 are classified in terms of the vortex type classification scale listed in Table 2-1. In addition, the swirl meter revolution rates are converted into swirl angles, which range from 11.7 to 14.5 degrees. As would be expected, the vortex type, swirl and swirl angle increase as the Reynolds number increases. The nature of the vortices is differ-

ent for the lower Reynolds number condition. However, the relationships between these vortices and the velocity distributions (at the inlet or near the intake) could not be defined for the three cases. Even though the details of the vortices are not fully characterized, these three flow scenarios still provide a series of experiments which will serve as a basis for comparison with CFD.

Table 4-1: Experimental Results

Expt ID	Q (m^3/s)	V (cm/s)	Re	Initial vortex location	Vortex Type	Swirl (rev/min)	Swirl angle (degrees)
1	0.0133	5.79	$2.4x10^4$	directly behind intake	1 to 2	28	11.7
2	0.0197	8.65	$3.6x10^4$	to right of intake	2 to 3	52	14.5
3	0.0237	10.32	$4.2x10^4$	to right of intake	3 to 5	60	13.9

5.0 Numerical Simulations

After completing a set of experiments covering a range of vortex conditions, a set of numerical simulations was completed using similar conditions. The experimental conditions were simulated using the FIDAP computational fluid dynamics (CFD) package. This chapter describes the FIDAP package and how it is used to develop model simulations.

5.1 The FIDAP Model

A number of computational fluid dynamic (CFD) codes are available commercially. Two of the more well known codes are the FLUENT code and the FIDAP package. FIDAP can simulate two and three-dimensional fluid flows, heat transfer, and mass transport (FIDAP 1993b). Program capabilities include incompressible and compressible flows, laminar and turbulent flows, and routines for incorporating a free surface. FIDAP is designed to perform all aspects of the model generation, problem setup, post-processing, and solution phases of a flow analysis.

5.2 Governing Equations

FIDAP was used, in this case, to solve the time averaged mass and momentum equations for incompressible turbulent flow. Conservation of mass is given by:

$$u_{j,j} = 0 \tag{5-1}$$

where u_j is the velocity and "j" indicates the gradient of u_j in the j direction. Momentum is given by:

$$\rho_o\left[\frac{\partial u_i}{\partial t} + u_j u_{i,j}\right] = -p_i + \rho_o f_i + \left[\mu\left(u_{i,j} + u_{j,i}\right) - \rho_o \overline{u_i u_j}\right]_j \tag{5-2}$$

where ρ_o is the fluid density, p_i is the pressure, f_i is gravitational acceleration, μ is the dynamic viscosity, $\rho_o u_i u_j$ is the Reynolds stress which represents the time-varying effects of turbulence on the mean flow.

For turbulence modeling the FIDAP package includes zero equation models, the standard κ-ε model, and a number of anisotropic models (including a Wilcox low Reynolds number κ-ω model) (FIDAP 1993a). For the base case flow condition, which was described earlier in Chapter 4 as the case with the flow rate of 0.0197m^3/s, the flow was initially modeled using the standard κ-ε model. For the standard κ-ε model the following parameters are used

$$\varepsilon = \nu \frac{1}{2} \overline{u_{i,j} u_{i,j}} \tag{5-3}$$

$$k = \frac{1}{2} \overline{u_i u_i} \tag{5-4}$$

where ε is the viscous dissipation of turbulent kinetic energy and k is the turbulent kinetic energy. From these equations the momentum equation can be rewritten in terms of a transport equation for k and another transport equation for ε.

$$\rho_o \left[\frac{\partial \varepsilon}{\partial t} + u_j \varepsilon_{,ij} \right] = \left[\mu_o + \frac{\mu_t}{\sigma_\varepsilon} \varepsilon_{,j} \right]_{,j} + c_1 \frac{\varepsilon}{k} \mu_t \Phi - \rho_o c_2 \frac{\varepsilon^2}{k} \tag{5–5}$$

$$\rho_o \left[\frac{\partial k_i}{\partial t} + u_i k_j \right] = \left[\mu_o + \frac{\mu_t}{\sigma_k} k_j \right]_j + \mu_t \Phi + \mu_t g_t - \rho_o \varepsilon \tag{5-6}$$

where μ_t is the turbulent dynamic viscosity given by $\rho_o c_\mu k^2/\varepsilon$, Φ is the viscous dissipation, and c_μ, σ_k, σ_ε, c_1, and c_2 are constants for which FIDAP provides recognized default values of 0.09, 1.00, 1.30, 1.44, and 1.92.

FIDAP provides a variety of options for defining elements and developing a mesh to discretize. For this project the governing equations were discretized over a mesh of 8 node iso-parametric brick elements, which was developed using the FI-GEN program (FIDAP 1993b). The model schematization was defined to simulate the physical model described previously.

5.3 Model Development

The FIDAP model serves as a tool that discretizes and solves these governing equations for specific geometries using a set of finite elements. This section describes the approach used to apply the FIDAP model to the pump intake problem, including the following items:

- Creating the mesh using the FI-GEN package
- Defining the boundary conditions using the FI-BC package
- Defining the equations to solve the simulation using the FI-PREP package
- Running the simulation using the FISOLV model solver

These steps are discussed in detail in the following sections. Appendix C contains a copy of the input that was used for the "base case" simulation.

5.3.1 Creating the Mesh

The mesh is created using the FI-GEN program. Use of the FI-GEN program first requires definition of the geometry for the model, followed by specification of the number of mesh points on the boundaries of the flow regime. FI-GEN then uses this information to generate the mesh.

The geometry of for the numerical model is obtained directly from the pump intake model that was used for the physical experiments. The dimensions of this model are shown in plan and profile in Figures 3-1 and 3-2 (from earlier) in Chapter 3. The dimensions are entered into the computer by typing in the coordinates of each point.

As noted above, once the geometry has been defined, the number of mesh points is specified for each of the boundary elements of the regime. Once this information has been defined, FI-GEN can be used to generate the mesh. FIDAP provides options for either a mapped mesh or a paved mesh. Mapped meshing is a regular checkerboard meshing. It is limited to four sided regions for surface areas and six sided regions for solids. Paved meshing is designed to automatically generate an all-quadrilateral mesh with qualities similar to those of the mapped mesh technique but without decomposition of the geometry. This is accomplished by layering or paving the geometry with rows or layers of quadrilateral elements from the boundary(ies) toward the interior. As rows begin to overlap or coincide at the interior of the geometry, they are carefully connected (sewn) together to form a valid quadrilateral mesh. Finally, an iterative cleanup and smoothing phase, where element deletion and/or addition takes place, is performed to improve the overall quality of the mesh.

For this application paved meshing was used to generate the mesh. The technique is relatively fast, robust, and capable of handling mesh transitions from small to large elements much more elegantly than mapping techniques. Furthermore, some characteristics of paved meshes include;

- Boundary sensitivity – Mesh contours closely follow the contours of the boundary. This characteristic is of particular importance for CFD applications due to the presence of boundary layers and the desire for well shaped elements in this area to capture boundary behavior.
- Orientation insensitivity – Rotating or translating a given geometry does not change the resulting mesh topology. A mesh generated in a transformed geometry is equivalent to the original mesh transformed.

- Few irregular nodes – An interior mesh node in an all-quadrilateral mesh is considered irregular if more or less than four elements are connected to it. This is a critical mesh topology feature because the number of elements sharing a node controls the final shape of the elements, even after smoothing. Thus a mesh with fewer irregular nodes, especially near the boundary where element shape is critical, is preferred.
- Transition ease – Transitioning between elements of varying size is critical for many CFD applications. Small elements must be placed in regions of large gradients to avoid excess discretization errors, while larger elements are more economical in areas of low gradients or where errors are less critical. Transitioning, of necessity, introduces more irregular nodes. Paving creates transitions automatically over short distances.
- Extendibility – Paving extends simply to general 3-D trimmed surfaces. Extension to all-hexahedral meshing of general 3-D solids, called plastering, is well under way.

The paving algorithm is available in FI-GEN for automatic meshing of any 3-D surface with almost no restriction on the region to be meshed. For these reasons the paved mesh approach was considered to be preferable. (FI-GEN manual 1993)

Figures 5-1 and 5-2 show plan and profile views, respectively, of the mesh that was used for the base case simulation. The mesh contains 24,949 elements, with approximately 80 elements in the x direction, 16 elements along the y direction, and 20 elements in the z direction. For simple geometries the mesh generation process is simple. However, for this case the pump intake is not a perfect cylinder. The intake includes a cylindrical section and a bellmouth flange at the inlet. To accommodate this complex geometry it was necessary to separate the model into separate regions in order to descretize the domain.

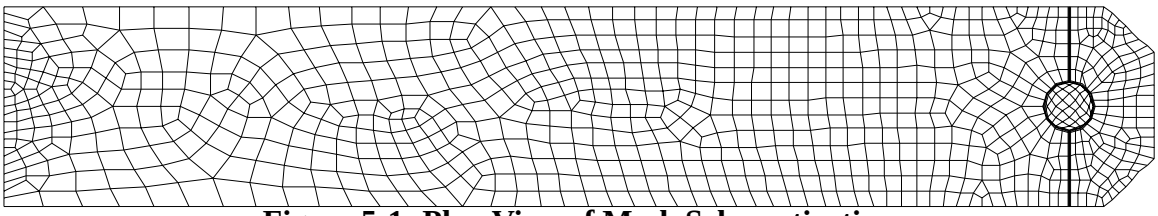

Figure 5-1: Plan View of Mesh Schematization

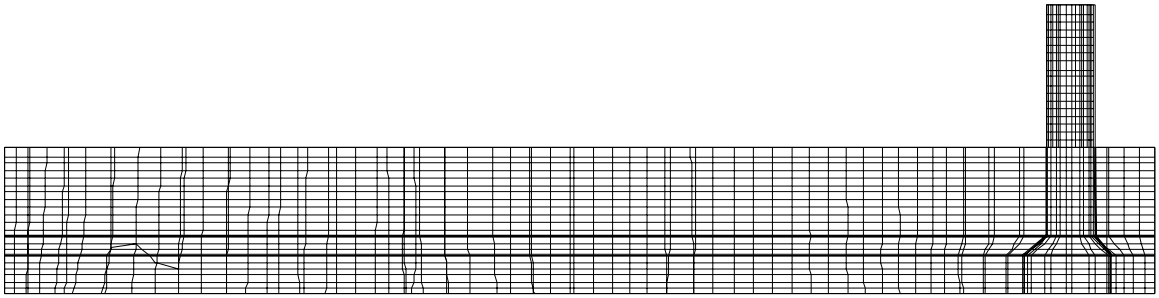

Figure 5-2: Profile View of Mesh Schematization

First, the model was divided into three levels. The first level contains the area below the bellmouth from elevations from 0 cm to 11 cm. The second level of the model consists of the bell of the intake. The bottom of this level is at an elevation of 11 cm and it extends to the top of the bell, which is located at 16.2 cm. The third level contains the top of the bell to the water surface. The depths contained within this level include 16.2 cm to 40.64 cm.

Next, each level of the model was separated into three separate regions. The first region is the area behind the intake, the second area is the intake itself or directly below the intake, and the final region is the area just upstream of the intake. These divisions produced nine sections of the model. Finally, an additional region was defined to contain the pump intake to a height of 80 cm above the tank.

All of the 10 regions are summarized in Table 5-1. Once the regions and number of nodes along each were specified, the FI-GEN package could be used to create a mesh in the model. A plan view of the model taken just below the water surface is shown in Figure 5-1. The mesh in this figure is denser in the area of the pump intake, which enables the program to make a better prediction of the flow characteristics in this area of the model. A profile of

the model taken along the centerline is shown in Figure 5-2. Heavy lines show the boundaries of the various regions in Figures 5-1 and 5-2.

Table 5-1: Descriptions of the areas of the computer model

Region #	Description of location
1	Area behind the pump intake z = 0 – 11
2	Area directly under the bellmouth z = 0 – 11
3	Area upstream of the pump intake z = 0 – 11
4	Area behind the pump intake z = 11 – 16.2
5	Area contained within the bell z = 11 – 16.2
6	Area upstream of the pump intake z = 11 – 16.2
7	Area behind the pump intake z = 16.2 – 40.64
8	Area within the intake pipe z = 16.2 – 40.64
9	Area upstream of the pump intake z = 16.2 – 40.64
10	Area of intake above the water level z = 40.64 – 80

5.3.2 Boundary Conditions

Once the mesh was defined, the next step is to assign boundary conditions to the model. Boundary conditions are defined using the FI-BC model. Using this package, values for densities, velocities, pressures, and other characteristics can be specified on the boundaries. For the purposes of this study, a constant value of density was specified for the entire model. The velocity distribution was assumed to be uniform at the inlet. For the base case simulation, the average velocity in the x-direction was 8.65 cm/s and the velocity in the y- and z-directions were zero. This description for the velocity distribution was sufficient to generate a flow in the system.

The FI-BC package is also used to designate which boundaries are solid walls and which are fluid. For this study all of the tank walls, including the water surface, and the pump intake were specified as solid walls by using the “wall” command. All other boundaries in the model were specified as fluid by using the “fluid” command.

5.3.3 Defining the Simulation Equations

The next step to set up a model using FIDAP is to signify the equation that will used to solve the model. The FI-PREP package is used to set up the equations that will be used to run the simulation and to further define the type of model. For this case, a steady state simulation with an incompressible, turbulent flow was set up using the problem command in the FI-PREP package.

The solution method that was used was a segregated solver with the segregated algorithm based on a pressure project specification. For this algorithm, each active degree of freedom is solved for sequentially and separately using the segregated solver. By using the pressure projection model, the pressure is solved for directly and a mass adjustment of the velocity field is performed at the end of each iteration to satisfy the incompressibility constraint. Therefore, the continuity equation is satisfied at the end of each iteration rather than when convergence is achieved.

5.3.4 Solving the Simulation

The FISOLV package is used to solve the simulation. The simulation may be run either in the foreground or the background. The simulations for this thesis were run in the background and convergence for the cases in this study was typically achieved within 320 iterations, with run times of approximately 24 hours on a DEC Alpha computer.

5.4 Numerical Modeling Comparison with Physical Experiments

Simulations were run using the three flow conditions that were established during the physical modeling experiments described in Chapter 4. Accordingly, the three cases that were modeled included:

1. the base case, which had a flow rate of 0.0197m^3/s,
2. the high Reynolds number case, which had a flow rate of 0.0237 m^3/s, and
3. the low Reynolds number, which had a flow rate of 0.0133 m^3/s.

Each simulation was compared to the physical model results which were summarized in Chapter 4.

5.4.1 Base Case

For the base case simulation, the flow rate entering the tank was 0.0197 m^3/s with a uniform velocity distribution of 8.65 cm/s at the inlet. These values provide a Reynolds number of 3.6×10^4. This velocity was chosen because, at this flow rate, Type 2 and 3 vortices (surface dimples and dye cores) were consistently present in the tank. As discussed in Section 5.2.1, the model contained 24,949 elements (as shown in Figures 5-1 and 5-2) and the simulation mode use of a standard κ–ε turbulence model. Finally, a slip condition was fixed on the bottom and boundary walls and left off of the top boundary to simulate a free surface.

Figures 5-3, 5-4, 5-5, 5-6, and 5-7, which are developed directly from FIDAP output processors, illustrate the results of the base case model simulation. In each of these figures the magnitudes of the velocity vectors (in cm/s) are indicated by the color scale and the length of each vector depends on the direction of the velocity. These figures are included for the purposes of this thesis to illustrate the basic features of model output. A more detailed set of figures showing plan views of velocity vectors near the pump intake can be found in Appendix D.

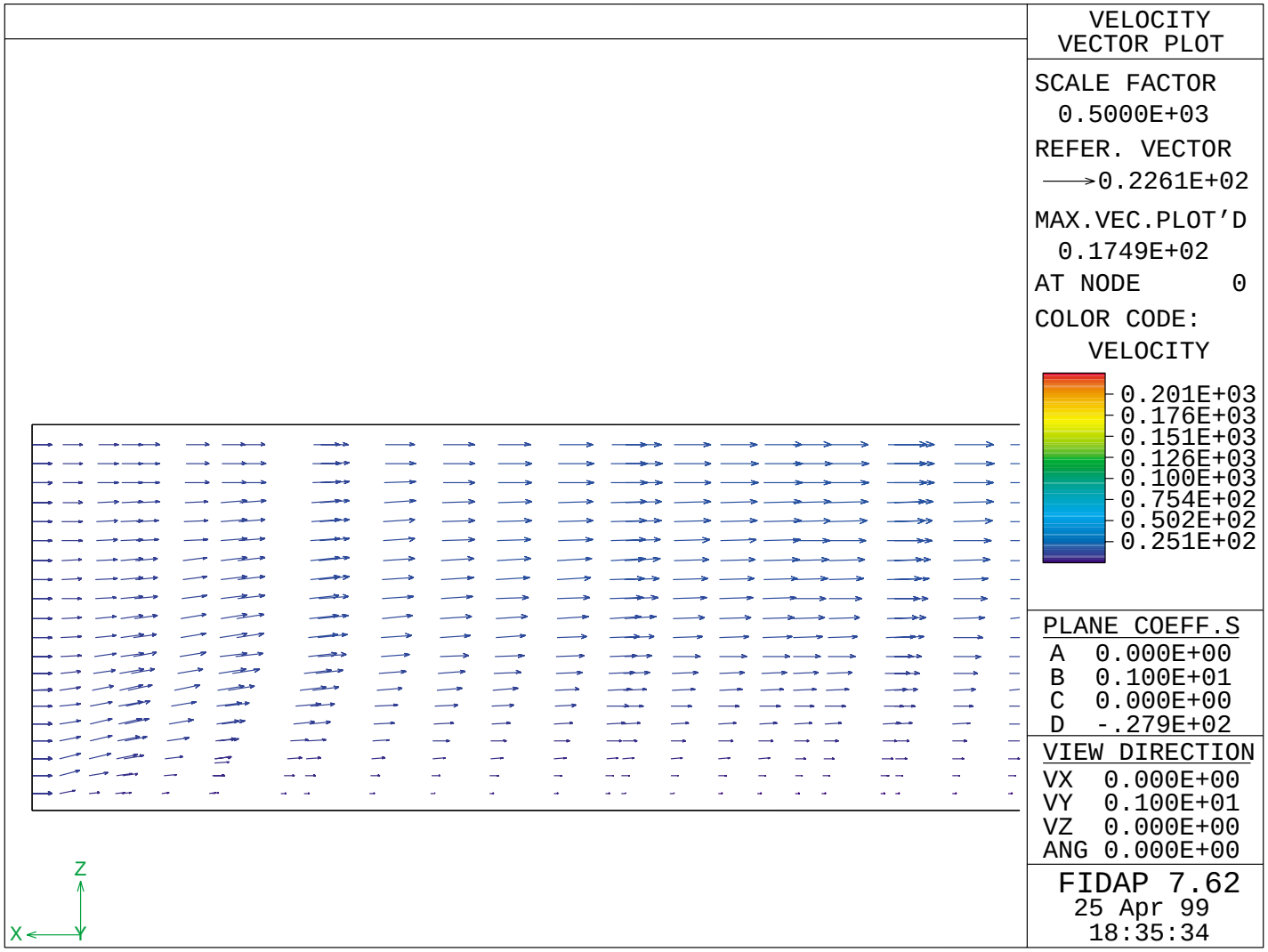

Figure 5-3: Velocity Vector Plot - Base Case (Re = 3.6 x 10^4) Profile View Taken along the Centerline Near the Inlet

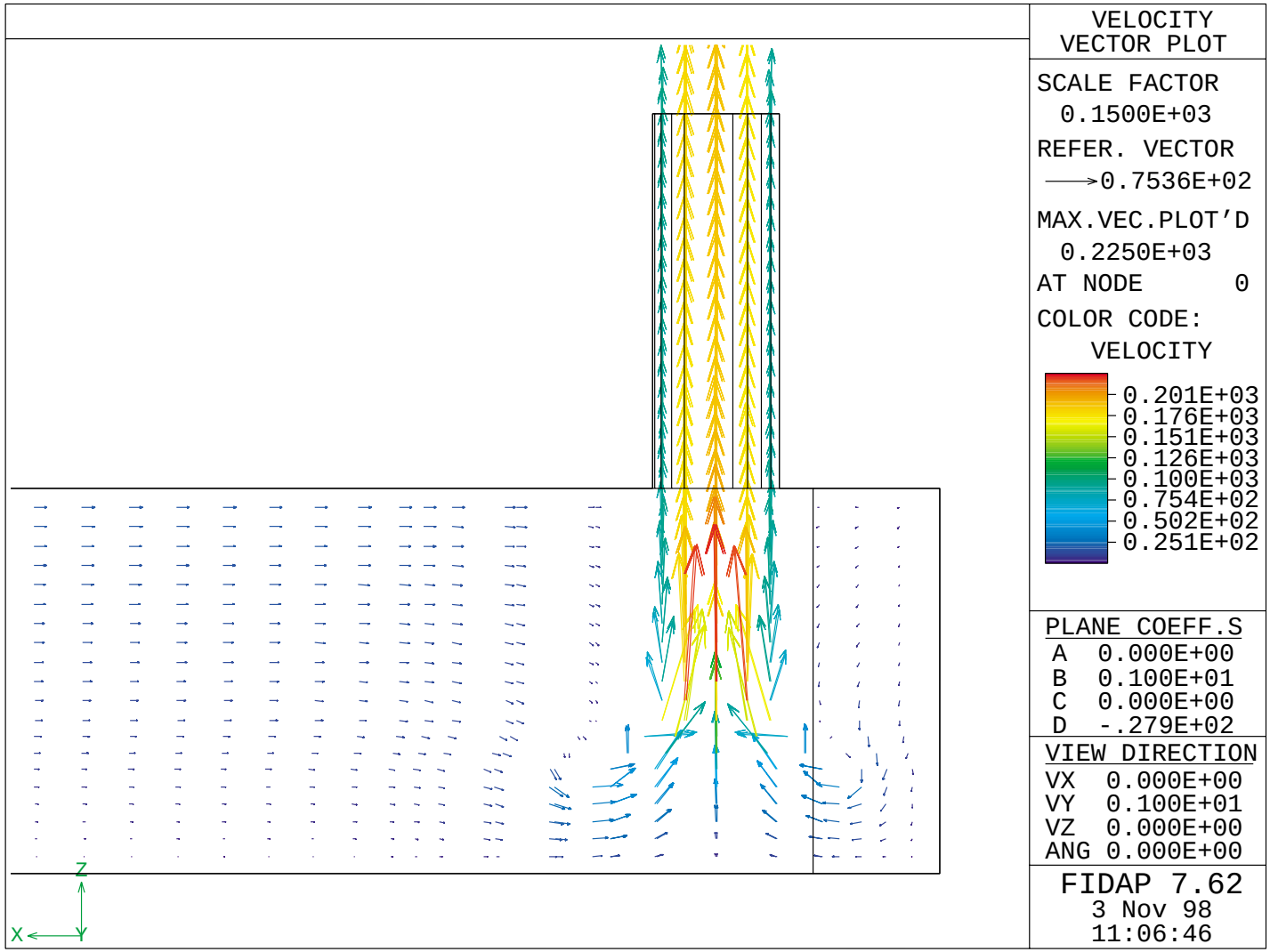

Figure 5-4: Velocity Vector Plot - Base Case (Re = 3.6 x 10^4) Profile View Taken along the Centerline Near the Intake

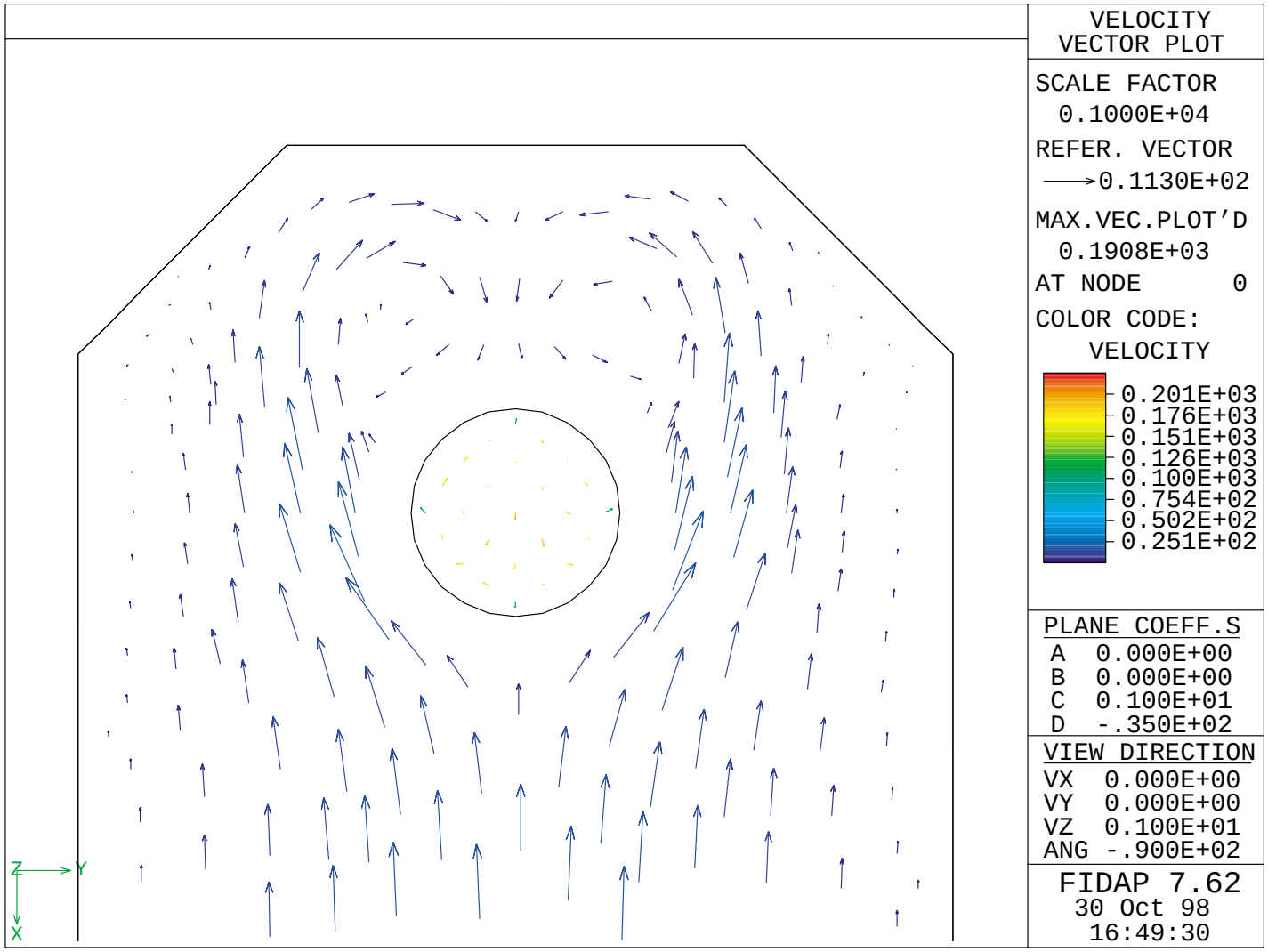

Figure 5-5: Velocity Vector Plot - Base Case (Re = 3.6 x 10^4) Plan View Taken at a Depth of 35 cm from the Tank Bottom

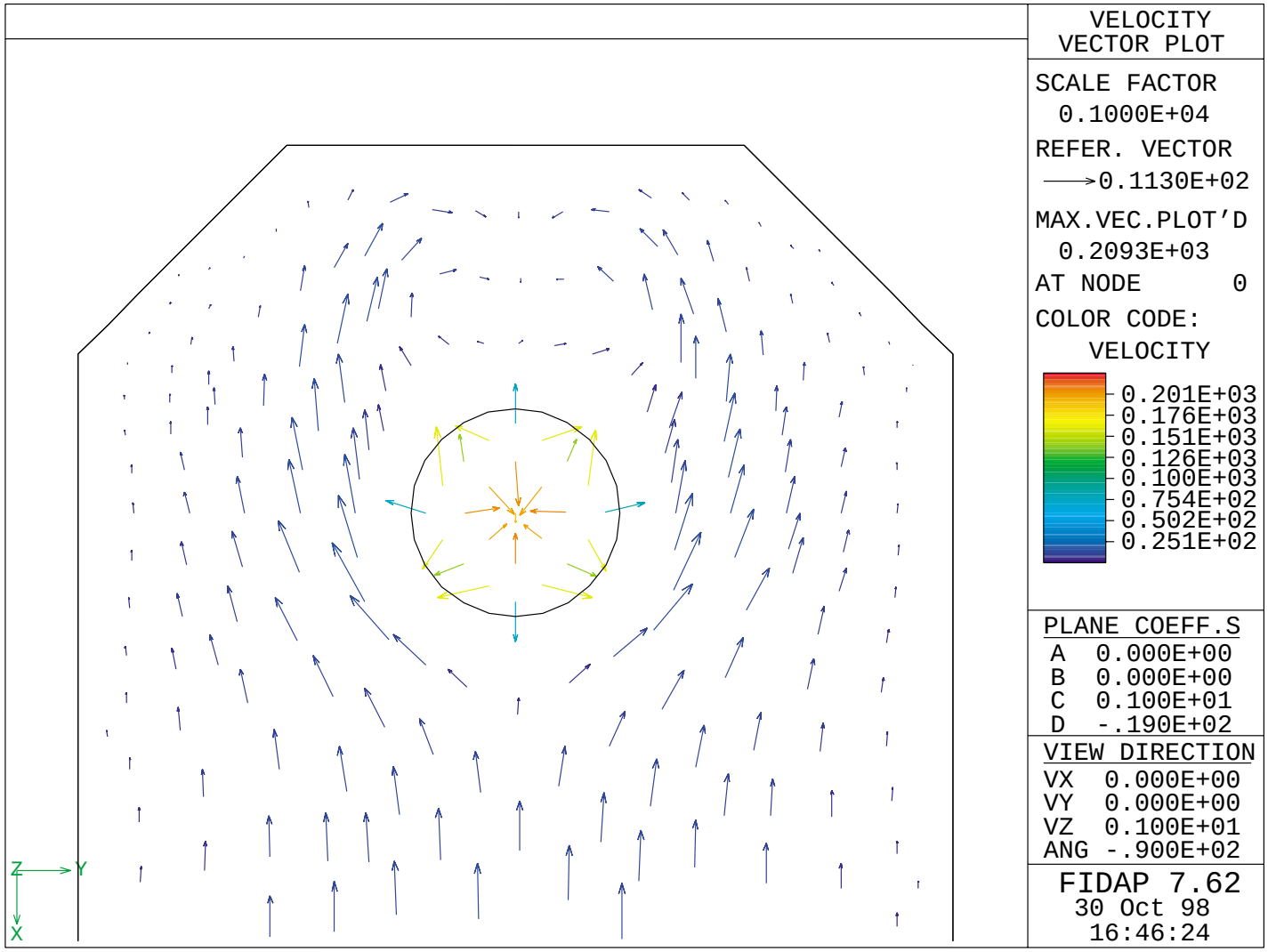

Figure 5-6: Velocity Vector Plot - Base Case (Re = 3.6 x 10^4) Plan View Taken at a Depth of 19 cm from the Tank Bottom

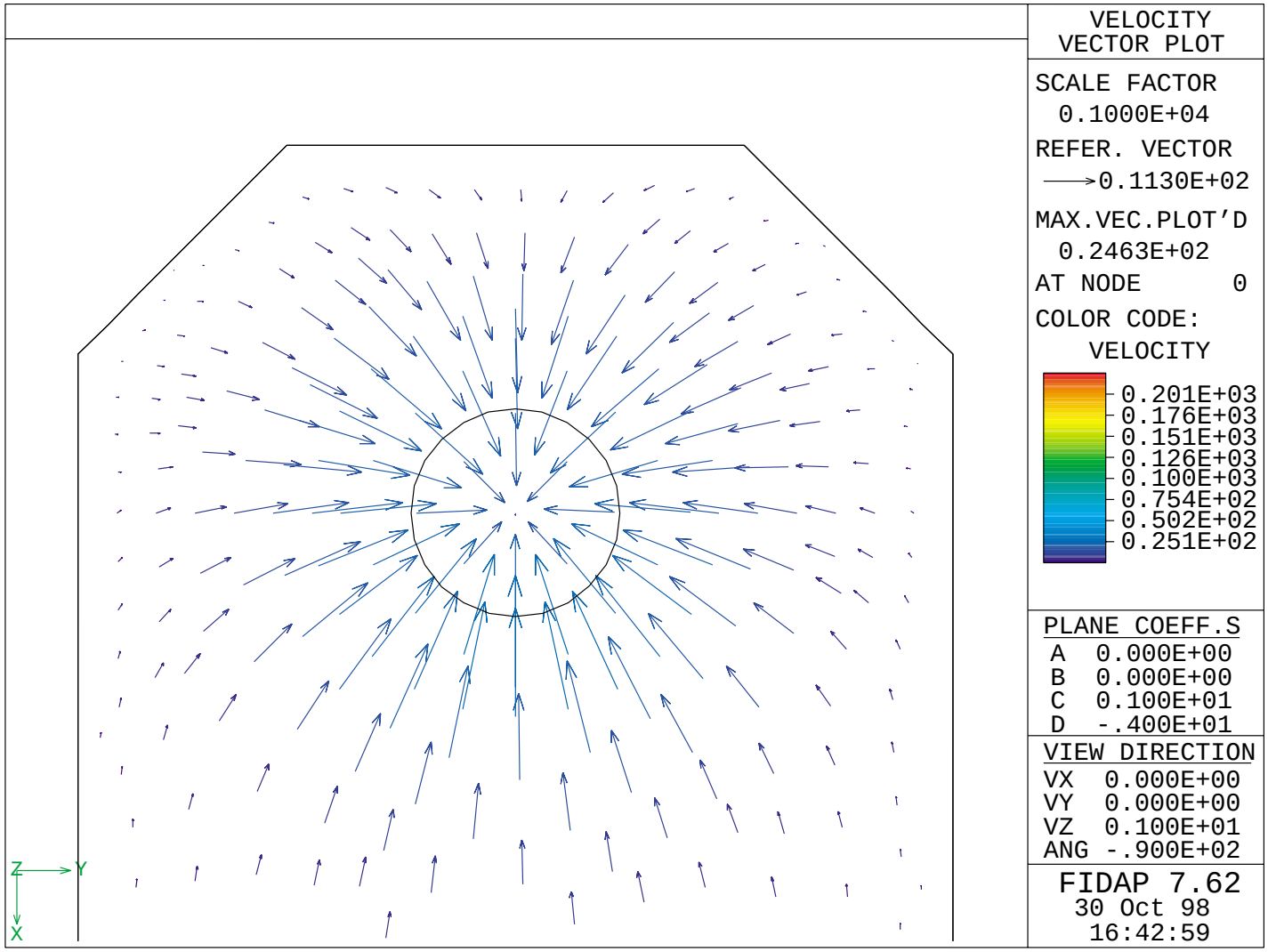

Figure 5-7: Velocity Vector Plot - Base Case (Re = 3.6 x 10^4) Plan View Taken at a Depth of 4 cm from the Tank Bottom

Figure 5-3 and 5-4 show profiles of the flow for the base case simulation. The profile in Figure 5-3 shows the uniform flow in the region upstream of the intake. This figure also illustrates the development of a boundary layer along the bottom wall of the region. For this simulation the approach flow remains uniform as it flows from the tank inlet to a location immediately upstream of the pump intake.

As the flow approaches the pump intake, the velocity distribution is affected due to the flow entering the pump. The nature of the flow in this region can be seen in Figure 5-4, which shows a profile view of the velocity vectors taken near the pump intake along the centerline of the tank. This figure shows that the approach flow is not drawn down towards the intake until it is in the immediate vicinity of the intake. The profiles in Figures 5-3 and 5-4 are consistent with expected circulation patterns that would be predicted by potential flow theory.

Figures 5-5, 5-6, and 5-7 show plan views of the intake at elevations of 35 cm, 19 cm, and 4 cm, respectively. The velocity vectors in Figure 5-5 (shown at an elevation of 35 cm) illustrate the circulation patterns near the water surface. Careful review of this figure reveals that two sets of counter-rotating vortices are apparent: one set is outside of the pump intake, and another is inside of the pump intake. For the region outside of the pump intake, the two counter-rotating vortices are symmetrically located directly behind the pump intake.

Vortices are also apparent in similar locations in Figure 5-6, which shows the velocity vectors at an elevation of 19 cm. This elevation is located immediately above the transition between the flange and the uniform cylindrical section of the intake. As would be expected, the vortices outside of the pump intake are slightly smaller than those shown in Figure 5-5. Inside the intake the vortices cannot be clearly seen and the flow is likely affected by the transition from the flange to the cylindrical section. Finally, Figure 5-7 shows a plan view of the velocity vectors for the flow at an elevation below the pump intake. This figure shows that flow is symmetrically directed towards the pump intake and no subsurface vortices are present.

An approximate estimate for the swirl associated with an individual vortex, n_v, can be obtained by determining the maximum tangential velocity in the vortex, v_m, along with its associated radius, r_m, and calculating a swirl rate as

$$n_v = v_m/(2\pi r_m) \tag{5-7}$$

and circulation as

$$\Gamma = 2\pi r_m v_m \tag{5-8}$$

This calculation yields an estimate of 3.8 for n_v and 11 cm^2/s for the circulation, which are both significantly lower than the values observed in experiments (which are listed in Table 5-2).

5.4.2 High Reynolds Number

The second case that was run was one with a high Reynolds number of 4.2×10^4. This case was chosen because the selected conditions matched those if the second case in the physical model experiments. As discussed in Chapter 4, Type 4 and 5 vortices consistently formed in the physical model experiments under this flow condition. This high Reynolds number simulation had a flow rate of 0.0237 m^3/s and a uniform velocity distribution of 10.44 cm/s at the inlet. Figure 5-8 shows a plan view of the velocity vectors at an elevation of 35 cm from the bottom of the tank. In this figure, two counter-rotating vortices can be seen both directly behind the pump intake and in the pump intake, which is similar to the flow pattern observed in the base case simulation. Thus, the locations and characteristics of the predicted vortices are essentially the same in the conditions as they were in the base case. The circulation and swirl rate inside the pump intake were also calculated for this simulation. The circulation was 22 cm^2/s and the swirl rate was 4.5 rev/min. As for the base case, these values are both significantly lower than the circulation and swirl rate values estmated for the physical experiments.

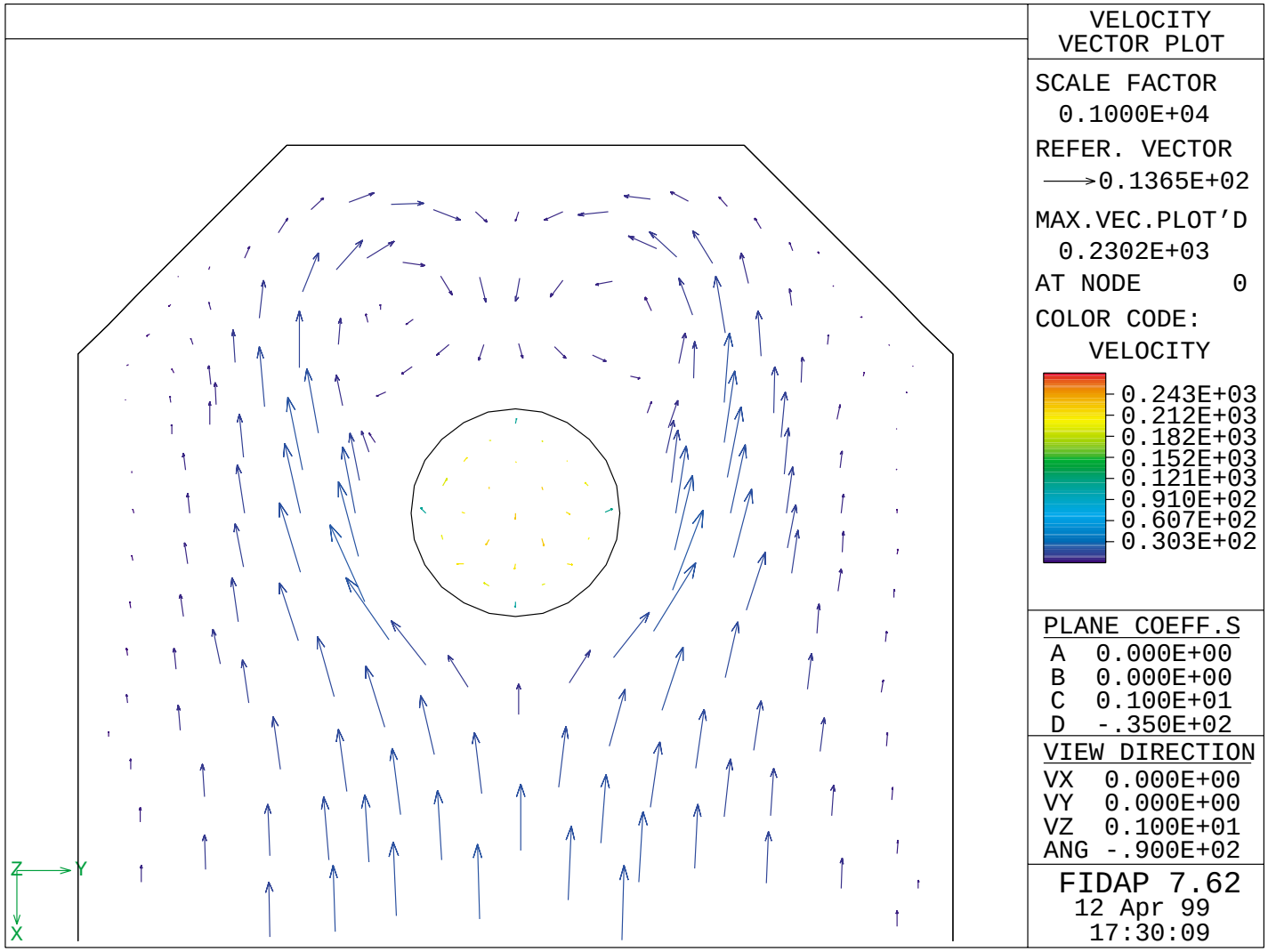

Figure 5-8: Velocity Vector Plot - High Reynolds Number (4.2×10^4) Plan View Taken at a Depth of 35 cm from the Tank Bottom

5.4.3 Low Reynolds Number

The final case to be used in the comparison of the physical and numerical modeling was the low Reynolds number case. This case had a Reynolds number of 2.4×10^4 and a uniform velocity distribution of 10.44 cm/s at the inlet. Figure 5-9 shows the plan view of the velocity vectors at an elevation of 35 cm from the bottom of the tank. Once again the locations and characteristics of the predicted vortices are essentially the same as those in the base case. Two counter-rotating vortices formed both directly behind the pump intake and inside the pump intake. However, in this case, the characteristics of the counter-rotating vortices observed in simulation results are significantly different than the experimental observations. While this difference may be a scale effect associated with the low Reynolds number use in this case, a full explanation of this difference is beyond the scope of this thesis. In the experimental results surface swirls were observed forming directly behind the intakebefore traveling to the right of the intake and dissipating.

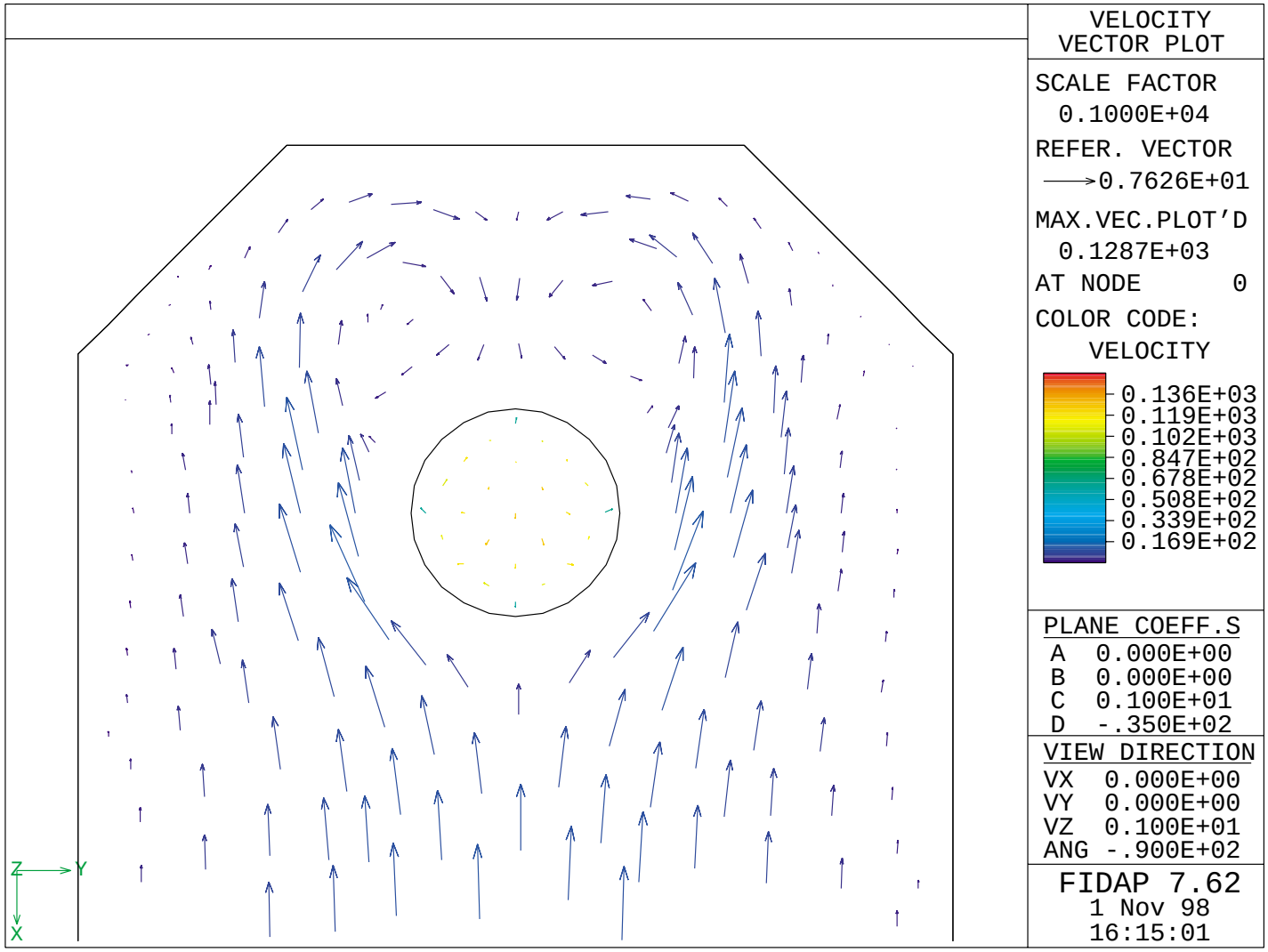

Figure 5-9: Velocity Vector Plot - Low Reynolds Number (2.4×10^4) Plan View Taken at a Depth of 35 cm from the Tank Bottom

5.4.4 Summary and Comparison with Experiments

The results of the simulations are summarized in Table 5-2. For each simulation, Table 5-2 includes some basic parameters defining the flow conditions (the flow rate Q, the average velocity of the approach flow V_{avg}, and the Reynolds number Re). Table 5-2 also includes descriptions of the predicted vortex type and location and approximate estimates for circulation, Γ, and swirl, n_v, associated with one of the vortices observed within the pump intake. The second row of this table is identified as the base case run since all additional simulations are compared directly with the results of the this simulation.

Vortices and swirling flow were apparent in all three simulations. As expected, circulation and swirl estimated for the simulation decreased as the Reynolds number decreased. However, in all three cases the values for circulation and swirl were smaller than the values obtained from the experiments.

Table 5-2: Results of the Base Case, High Re, and Low Re Flow Conditions

Description	Q (m3/s)	Vavg (cm/s)	Reynolds Number	Circulation (cm2/s)	Swirl Rate (rev/min)	Vortex Type and Location
Low Re	0.0133	5.85	2.4 x 104	11	2.5	same as base case
Base Case	0.0197	8.65	3.6 x 104	18	4	2 counter-rotating vortices behind and inside of intake
High Re	0.0237	10.44	4.2 x 104	22	4.5	same as base case

The nature and location of the vortices in the simulations closely match the simulation results obtained for a similar configuration by Constantinescu and Patel (1998). In addition, as discussed in Chapter 4 vortices were were also observed in the pump intake model for the same flow conditions as this simulation. However, review of the experimental observations shows that one vortex followed a cyclical drifting pattern in the tank on the right side of the pump intake. While the initial location of the observed vortices in the

experiment is close to the predicted location for one of the vortices predicted by the model, the model simulations do not include any time dependency and the available information is therefore insufficient to draw any conclusions regarding this similarity.

5.5 Sensitivity Analysis

As a step to initiate a more detailed modeling effort, a number of simulations were completed to develop an indication of the sensitivity of the model results to the parameters, schematization and assumptions used to develop the model. These analyses are not intended to fully address the sensitivity associated with every component of the model. Rather, they are intended to demonstrate some bounds on model predictions and thereby establish a basis for more detailed modeling approach. The specific runs include simulations to:

- investigate the role of Reynolds number
- investigate the effect of schematization
- investigate the role of the turbulence model
- define the role of the inlet velocity distribution
- assess the importance of the boundary condition on the free surface

5.5.1 Role of Reynolds Number

The three simulations summarized in the previous section effectively provide a demonstration of the effects of Reynolds number. The results of the simulations for the three Reynolds numbers were similar. The cases all had similar flow patterns with two sets of counter-rotating vortices forming behind and inside of the pump intake. The circulation and swirl rates that were measured differed with the Reynolds number as expected.

5.5.2 Effects of Schematization

In the initial development of the model, simulations were completed using a coarse mesh consisting of 8,624 nodes. The results of these earlier runs are included here to illus-

trate the importance of model schematization for this case. The mesh is shown in Figure 5-10. The flow rate for this simulation was 0.0197 m^3/s and the velocity used was a uniform velocity distribution of 8.65 cm/s. These conditions matched the base case condition and gave a Reynolds number of 3.6×10^4. A standard k-e turbulence model was used.

Figure 5-11 shows a plan view of the velocity vectors at an elevation of 35 cm. This simulation again produced two counter-rotating vortices behind and inside the pump intake. The circulation and swirl rate for this model were 51 cm^2/s and 14 rev/min. Due to the coarseness of the mesh, it was difficult to clearly define the swirl in the pump intake and to accurately determine the circulation for this case. However, the circulation value again differed significantly from the value of 52 rev/min, observed in the base case physical model experiments. By reducing the number of elements, the results of the simulation were similar to the results of the base case simulation. However, the flow patterns were more difficult to define and therefore the calculated circulation values may not be as accurate as those that were obtained in the base case.

Since the coarse mesh model and the base case model yield equivalent flow patterns, the results provide some verification that the base simulation provides adequate resolution for resolving vortices. As seen in Figure 5-11, however, with a fewer number of elements it becomes more difficult to clearly define the characteristics of the flow. Constantinescu and Patel (1998) note the appearance of additional fine vortices along the outside of the pump intake. These vortices are most likely not observed in this case or the base case simulation because the discretization of the mesh is too coarse to resolve these vortices. While an increased mesh resolution would likely improve the representation of finer-scale flow features, the base case resolution likely is sufficient to capture the basic flow patterns.

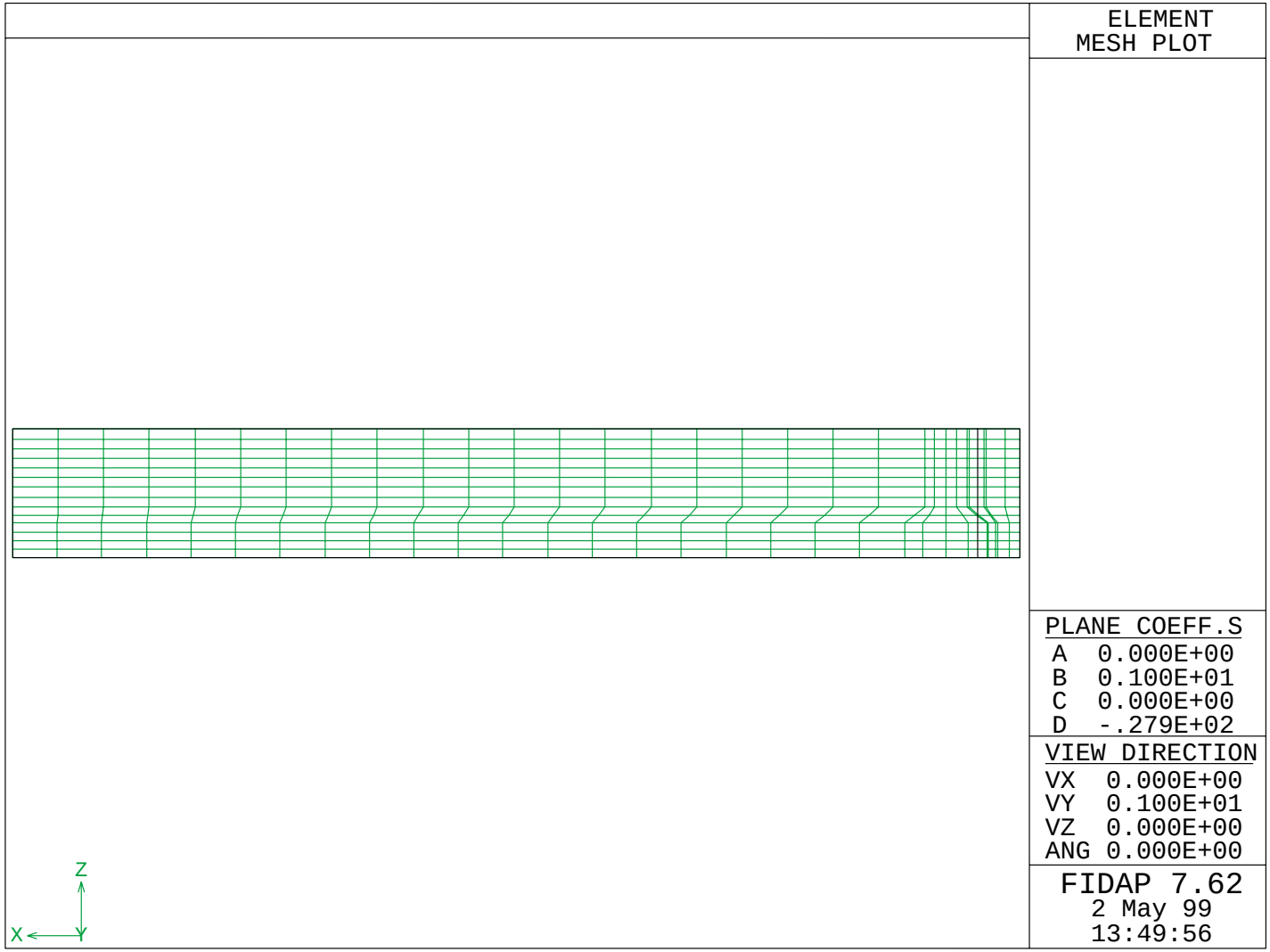

Figure 5-10: Profile View Taken Along the Centerline for the Coarse Mesh

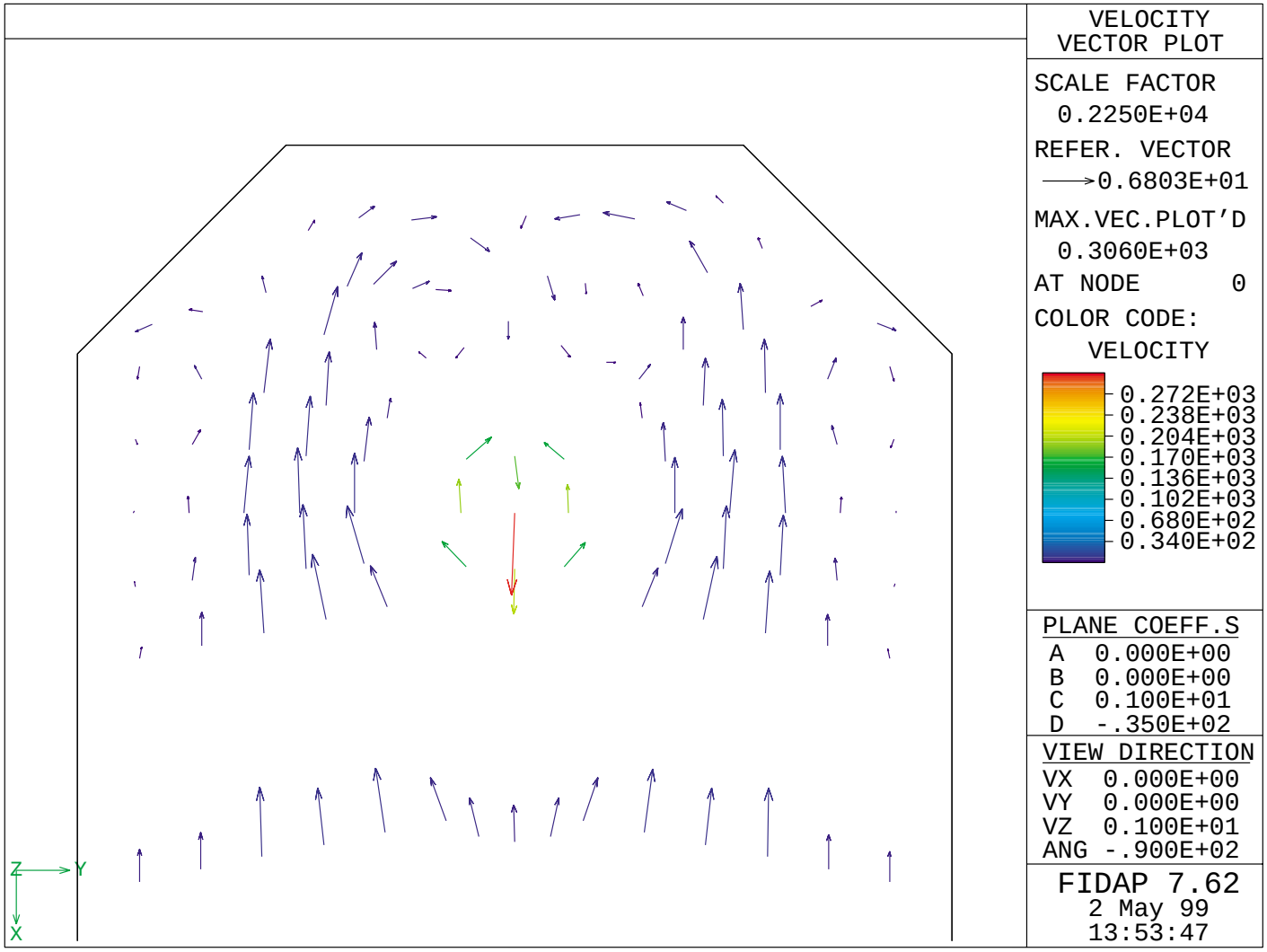

Figure 5-11: Velocity Vector Plot - Coarse Mesh Plan View Taken at a Depth of 35 cm from the Tank Bottom

5.5.3 Role of the Turbulence Model

Since it is known that swirling flows often are anisotropic in nature, an anisotropic k-e model is also used to simulate the flow. The model employed makes use of specialized approaches following Launder (1990) and Speziale (1990) to obtain the coefficients c_1 and c_2. Figure 5-12 shows a plan view of the velocity vectors at an elevations of 35 cm. When the anisotropic κ–ε model was used, two counter-rotating vortices were still evident at the same location both outside of and within the pump intake, and the results were qualitatively the same as those of the base case. The flow patterns in this case are similar to those of the base case, shown in Figure 5-5; however, the vortices are slightly off center, to the left of the intake. In addition, as can be seen in Table 5-3, the estimated circulation and swirl for an individual vortex within the pump intake are reduced by a factor of 2 when the anisotropic k-e model is used rather than the standard κ–ε model.

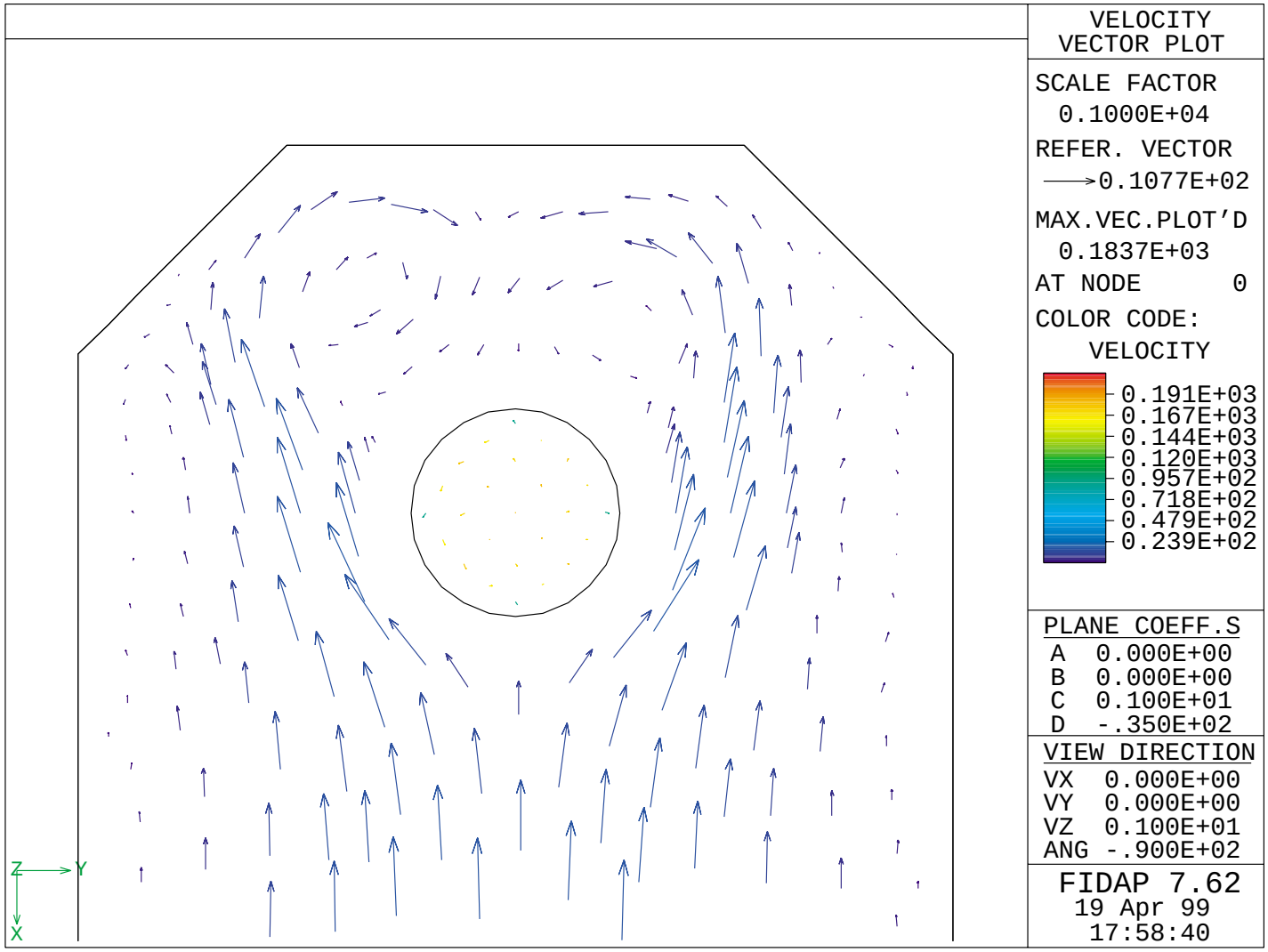

Figure 5-12: Velocity Vector Plot - Anisotropic Turbulence Model. Plan View Taken at a Depth of 35 cm from the Tank Bottom

5.5.4 Effects of Boundary Conditions

5.5.4.1 Role of Approach Flow

Since the approach flow is known to have a significant impact on vortex development, the role of the inlet boundary condition (leading to a different flow condition) was considered. A linear velocity gradient in z was investigated in which the Reynolds number (based on average velocity) was maintained at 3.6×10^4 but the velocity was defined as $U = (17.3/41)z$. Figure 5-13 shows the velocity profile at the inlet. This case provided an upper bound on the potential role of vertical shear. Again this run yielded only slight changes in the vortex locations, as can be seen in Figure 5-14. However, as expected, the circulation and swirl increased significantly due to the increased shear in the approach flow. The circulation was 104 cm^2/s and the swirl rate was 15 rev/min.

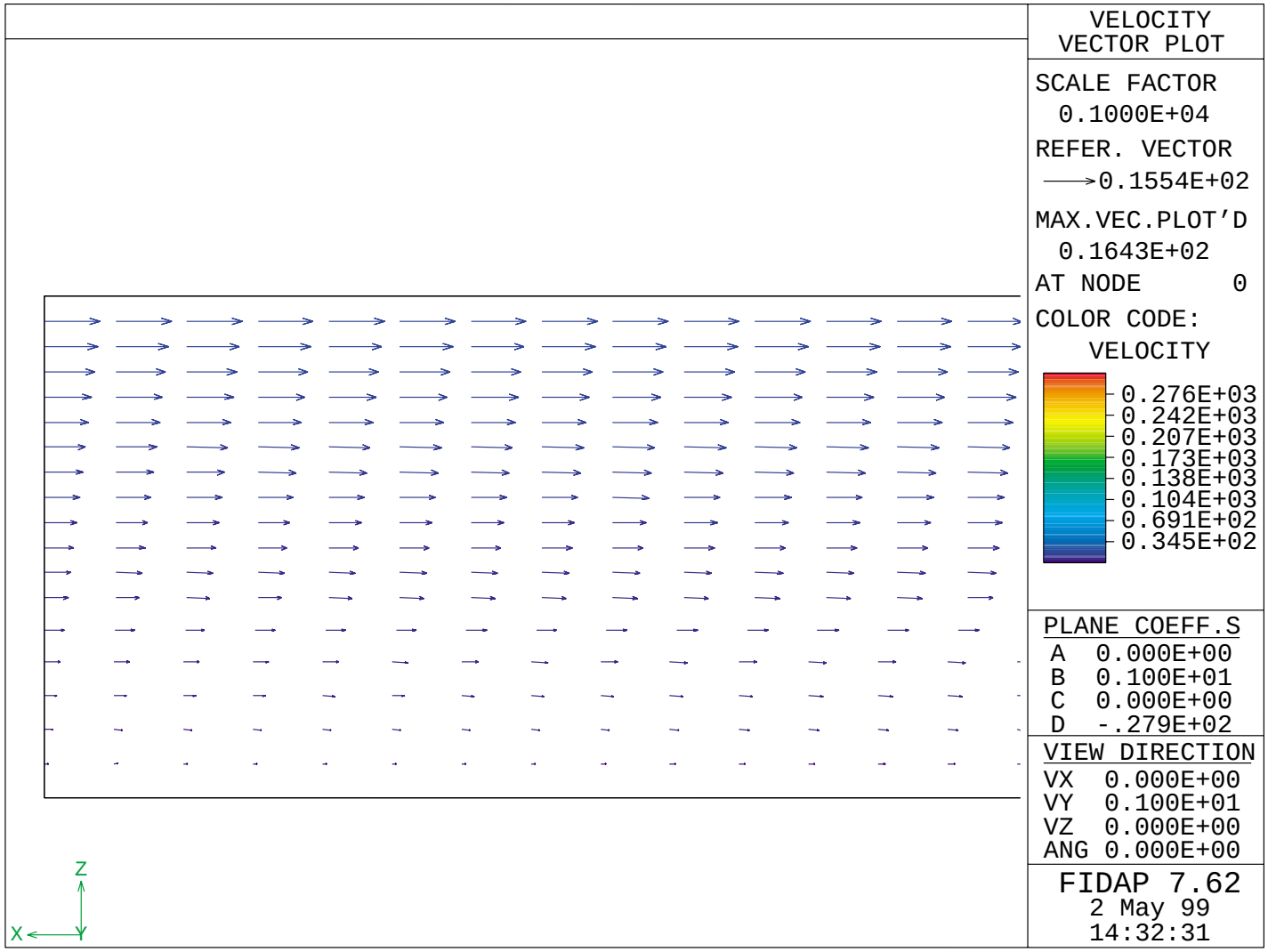

Figure 5-13: Velocity Vector Plot - Linear Inlet Velocity Profile Profile View Taken along the Centerline

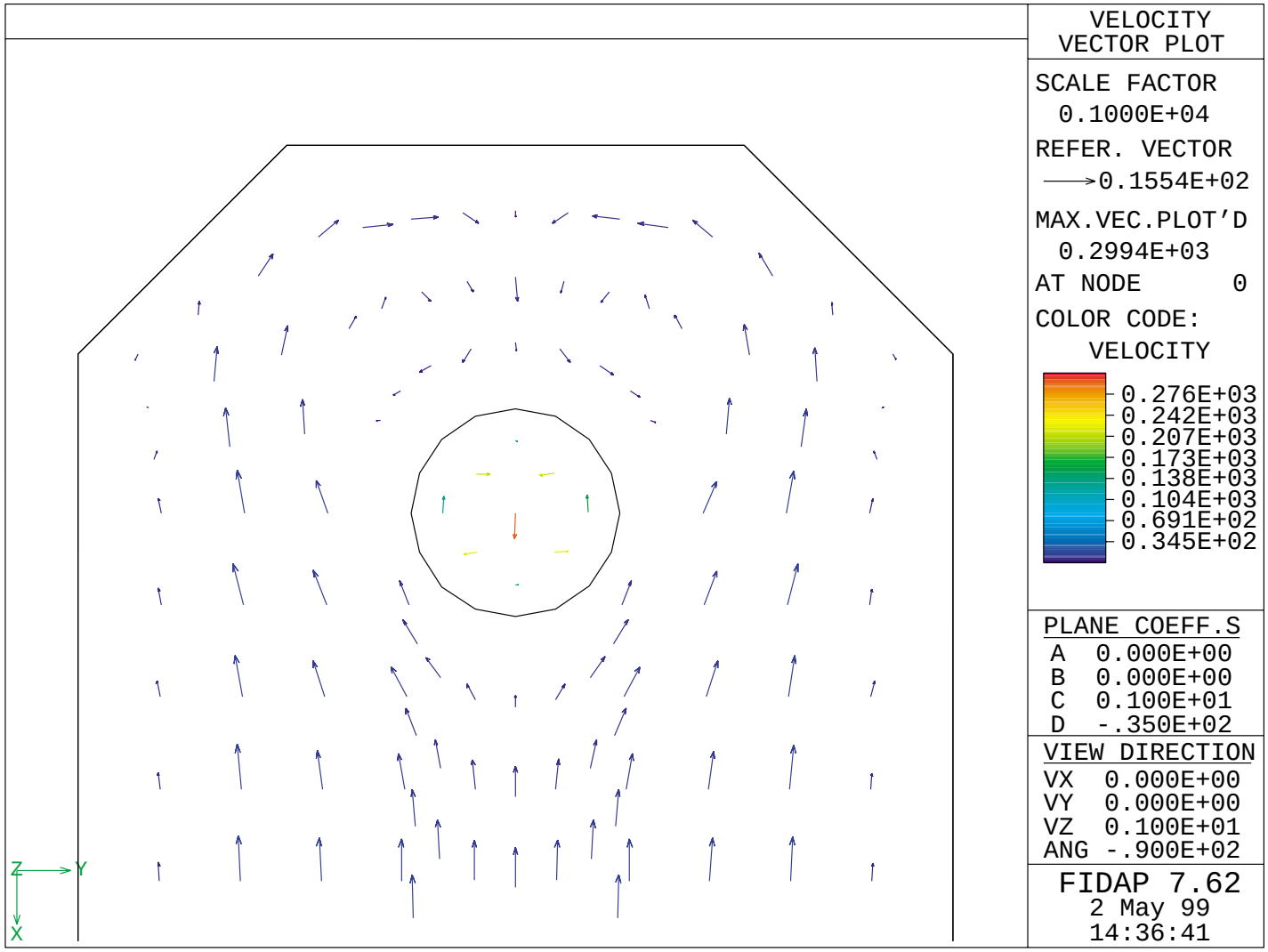

Figure 5-14: Velocity Vector Plot - Linear Velocity Profile Plan View Taken at a Depth of 35 cm from the Tank Bottom

5.5.4.2 Role of Slip Condition on the Boundary

To assess the importance of the surface boundary condition, FIDAP's input was adjusted such that a no-slip condition existed on the surface. Figure 5-15 shows a velocity profile along the centerline. While this adjustment had only minor effects on the locations of the vortices (as for all previous cases), the circulation and swirl increased by more than a factor of three as a result of the increased shear introduced to the approach velocity profile. The vortices can be seen in Figure 5-16.

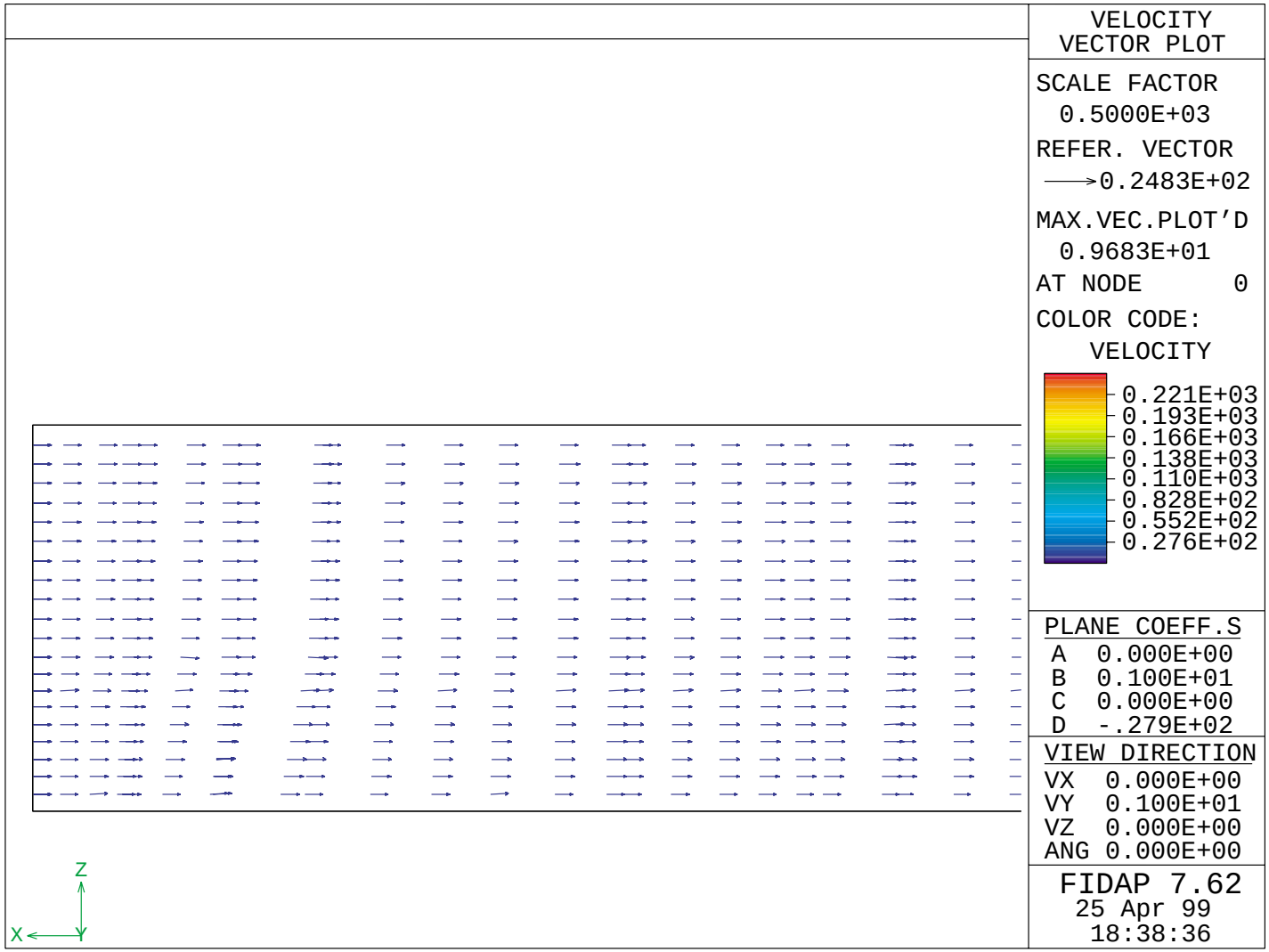

Figure 5-15: Velocity Vector Plot - Profile Taken along the Centerline for the No-Slip Condition

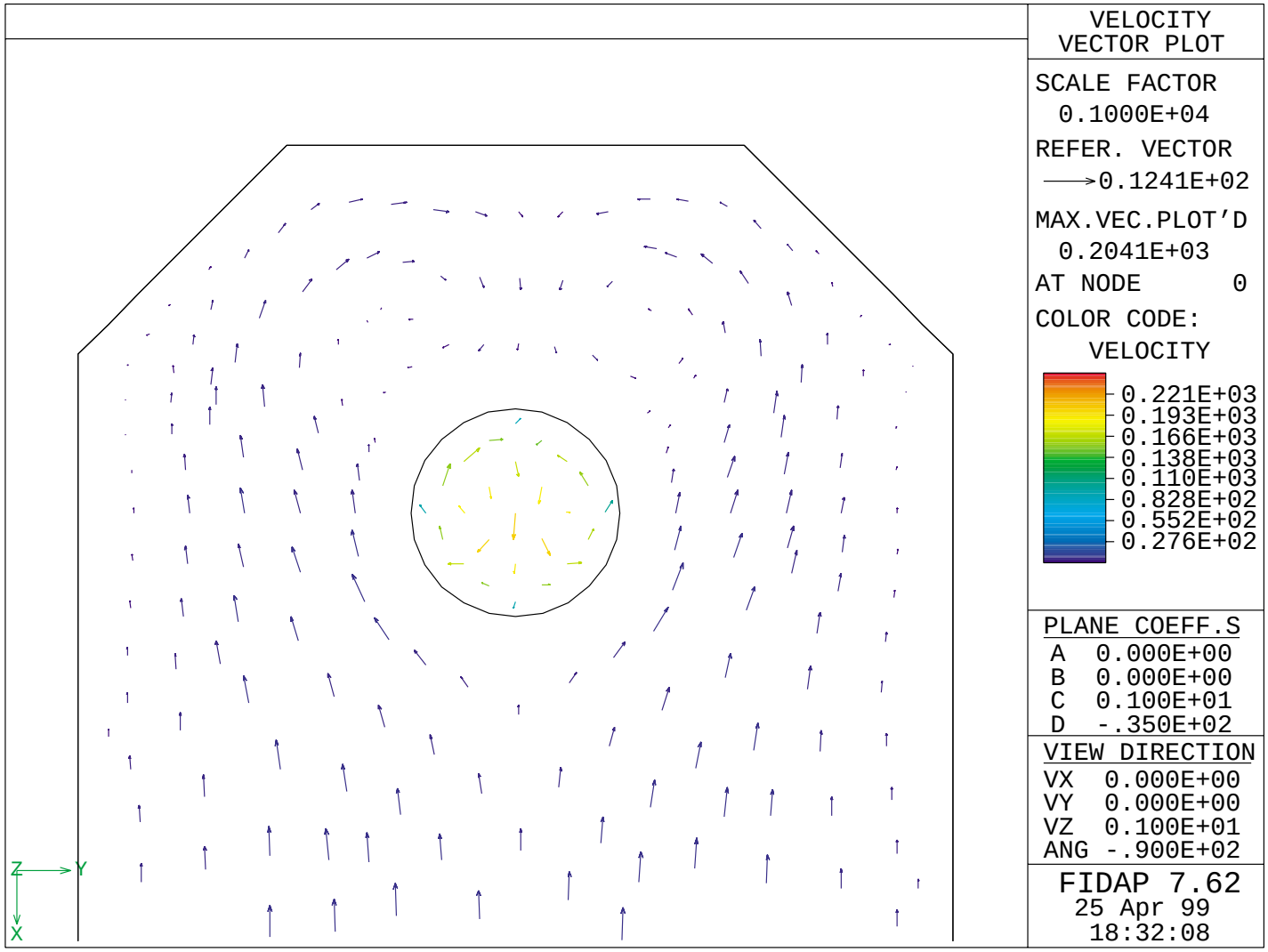

Figure 5-16: Velocity Vector Plot - No-Slip Condition Plan View Taken at a Depth of 35 cm from the Tank Bottom

5.5.5 Summary

All of the results of the sensitivity analyses are summarized in Table 5-3. For a number of these sensitivity simulations circulation and swirl rate increased significantly. however, for all of these simulation runs, the basic flow patterns remained the same. A more extensive modeling effort is necessary to fully understand the differences between the results of the simulations and the experiments.

Table 5-3: Results of the Computer Simulation

Description	Q (m^3/s)	V_{avg} (cm/s)	Reynolds Number	Circulation (cm^2/s)	Swirl Rate (rev/min)	Vortex Type and Location
Base Case (std. κ–ε model, uniform inflow, 24,949 elements						
Conditions defined from experiments	0.0197	8.65	$3.6x10^4$	18	4	2 counter-rotating vortices behind and inside of the intake
Effects of Reynolds Number						
Low Re	0.0133	5.85	$2.4x10^4$	11	2.5	Same as base case
High Re	0.0237	10.44	$4.2x10^4$	22	4.5	Same as base case
Effects of schematization						
8624 elements	0.0197	8.65	$3.6x10^4$	51	14	Same as base case
Role of Turbulence Model						
Anisotropic κ–ε	0.0197	8.65	$3.6x10^4$	9	2	Same as base case
Effects of Boundry Conditions						
Linear velocity profile at inlet (17.3/41)z	0.0197	8.65	$3.6x10^4$	104	15	Same as base case
No slip for the surface boundary	0.0197	8.65	$3.6x10^4$	62	14	Same as base case

6.0 Conclusions

This thesis describes a project intended to assess the use of computational fluid dynamics (CFD) software to resolve the fluid dynamics in the vicinity of a pump intake. Experiments were developed in a pump intake model to observe the qualitative aspects of vortices adjacent to a pump intake. as summarized in Chapter 4, free surface vortices of varying strengths were observed for all experiments completed. These experiments served as the basis for numerical model development and simulations completed to investigate the applicability of commercially-available CFD software to address the pump intake problem.

The numerical simulations were developed using the same flow conditions and geometry as those used in the physical model predicted the occurrence of vortices that are similar in nature to those predicted by Constantinescu and Patel (1998). However, these predictions include dual counter-rotating vortices within the intake and in the flume adjacent to the intake. Experimental observations revealed single vortices within the intake and single vortices developing in the flume on one side of the intake. Furthermore, estimates of circulation and vorticity for vortices predicted by simulations are consistently lower than those observed in experiments. While slight non-uniformities in the approach flow or possible constraining effects of the swirl meter in the intake could provide some explanation for these differences, limitations in the numerical application are considered to be a more likely explanation.

Consequently, a series of sensitivity analyses were completed to assess the significance of some basic model assumptions relative to the vortex predictions. These simulations indicate that the selection of the schematization, turbulence model, approach flow characteristics, and model boundary conditions (e.g. the free surface boundary conditions) can affect the intensities of predicted vortices. The effects of shear introduced through the top boundary conditions and inlet boundary condition do have

importance effects on the circulation and swirl. However, within the context of the current model application, these effects do not appear to resolve the discrepancy between predicted and observed vortex characteristics.

Consequently, this thesis is considered to be a first step in investigating the practical application of available CFD codes to address vortex development, and additional analyses are necessary. These analyses include comparisons with other on-going modeling efforts, more detailed characterization of spatial variability in the approach flow, consideration of a free surface boundary condition, and evaluation of the effects of temporal variability. In addition, since this numerical model application only provides a time-averaged representation of the effects of the time-varying turbulence on the mean flow, the model cannot fully capture the effects of any temporal variability. Since the experimental results clearly indicated a time-varying nature of the observed vortices, future analyses are needed to address stability and to develop simulations accommodating time-variations or perturbations in the mean flow.

Appendix A - Directions for running the pump intake model at ARL

1) Fill tank

Materials needed

- extension cord
- sump pump - if the sump pump is not at the tank, then obtain a sump pump from an ARL employee

i) drop the pump into the sump near the tank
ii) place hose connected to the sup pump in the tank
iii) plug an extension cord into the electrical outlet behind the tank
iv) plug the sump pump's plug into the extension cord to turn on the sump pump
v) use the sump pump to fill tank to desire water level and unplug the pump

2) Fill the intake pipe with water

Materials needed

- vacuum pump
- large glass bottle
- rubber stopper (2 holes)
- plastic tubing

i) connect tubing from the top of the intake pipe one of the holes in the rubber stopper
ii) place rubber stopper in the glass bottle
iii) connect vacuum pump to the glass bottle with plastic tubing
iv) place one end of the tubing in the remaining hole of the rubber stopper, connect the other end of the tubing to the vacuum pump
v) plug the vacuum pump into the extension cord until the intake pipe is full of water, (water will begin to fill the glass bottle when this happens)
vi) once the pipe is full unplug the vacuum pump
vii) if the water level in the tank is not at the desire height, fill the tank according to the above directions

3) Start pump

- sometimes the pump cannot be operated when other models are in use, the ARL workers will typically tell you when this is a problem

i) push the green pump start button, this should be located on the side of the tank
ii) open the valve on the pump by turning it counter clockwise, until the desired flowrate is reached
iii) adjust the water level if necessary using the sump pump

4) Stop pump

i) close the valve on the pump by turning it clockwise
ii) push red stop pump button

Appendix B - Photos

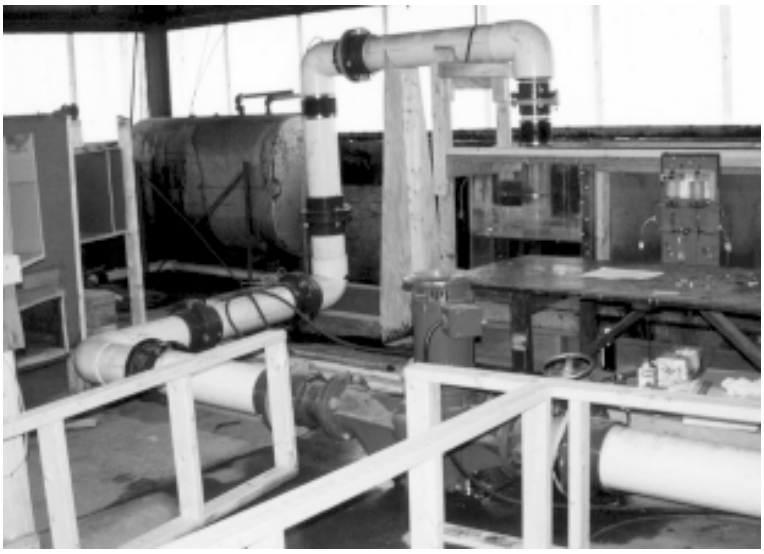

Pump Intake

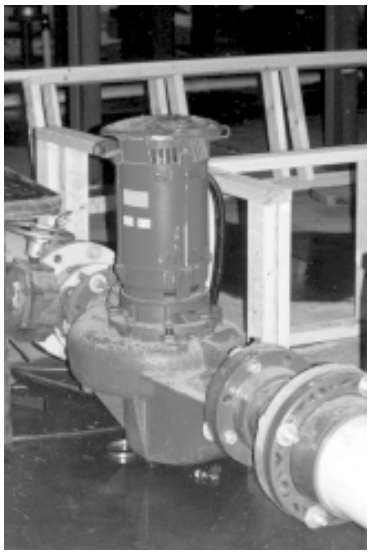

Pump

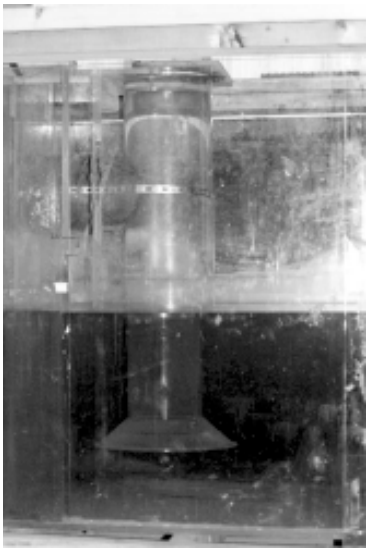

Pump Intake

Pump Intake Model

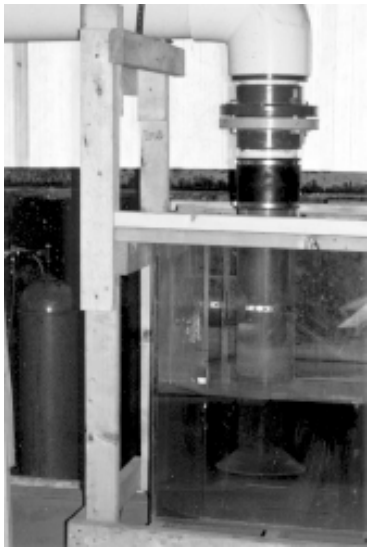

Bellmouth

Appendix C - Input File for FIDAP

C.1 Geometry Definition in FI-GEN

```
FI-GEN( ELEM = 1, POIN = 1, CURV = 1, SURF = 1, NODE = 0, MEDG = 1, MLOO = 1,
MFAC = 1, BEDG = 1, SPAV = 1, MSHE = 1, MSOL = 1, COOR = 1 )
POINT( ADD, SHOW, COOR, X = 0, Y = 13.335 )
POINT( ADD, SHOW, COOR, X = 0, Y = 42.545 )
POINT( ADD, SHOW, COOR, X = 13.335, Y = 0 )
POINT( ADD, SHOW, COOR, X = 13.335, Y = 55.88 )
POINT( ADD, SHOW, COOR, X = 23.495, Y = 0 )
POINT( ADD, SHOW, COOR, X = 23.495, Y = 55.88 )
POINT( ADD, SHOW, COOR, X = 318.135, Y = 0 )
POINT( ADD, SHOW, COOR, X = 318.135, Y = 55.88 )
POINT( ADD, SHOW, COOR, X = 23.495, Y = 14.9225 )
POINT( ADD, SHOW, COOR, X = 36.5125, Y = 27.94 )
POINT( ADD, SHOW, COOR, X = 23.495, Y = 40.9575 )
POINT( ADD, SHOW, COOR, X = 10.4775, Y = 27.94 )
POINT( SELE, LOCA, WIND = 1 )
/ ID = 1
/ ID = 2
CURVE( ADD, LINE )

POINT( SELE, LOCA, WIND = 1 )
/ ID = 1
/ ID = 3
/ ID = 5
/ ID = 7
CURVE( ADD, LINE )

POINT( SELE, LOCA, WIND = 1 )
/ ID = 2
/ ID = 4
/ ID = 6
/ ID = 8
CURVE( ADD, LINE )

POINT( SELE, LOCA, WIND = 1 )
/ ID = 7
/ ID = 8
CURVE( ADD, LINE )

POINT( SELE, LOCA, WIND = 1 )
/ ID = 9
/ ID = 10
/ ID = 11
CURVE( ADD, CIRC )

CURVE( SELE, LOCA, WIND = 1 )
/ ID = 9
/ ID = 10
```

```
CURVE( SPLI )

CURVE( SELE, LOCA, WIND = 1 )
/ ID = 11
/ ID = 11
CURVE( SPLI )

CURVE( SELE, LOCA, WIND = 1 )
/ ID = 13
/ ID = 12
CURVE( SPLI )

POINT( SELE, LOCA, WIND = 1 )
/ ID = 6
/ ID = 11
CURVE( ADD, LINE )

POINT( SELE, LOCA, WIND = 1 )
/ ID = 5
/ ID = 9
CURVE( ADD, LINE )

CURVE( SELE, LOCA, WIND = 1 )
/ ID = 8
MEDGE( ADD, SUCC, INTE = 30, RATI = 0, 2RAT = 0, PCEN = 0 )

MEDGE( SELE, LOCA, WIND = 1 )
/ ID = 1
MEDGE( MODI, SUCC, INTE = 24, RATI = 0, 2RAT = 0, PCEN = 0 )

MEDGE( SELE, LOCA, WIND = 1 )
CURVE( SELE, LOCA, WIND = 1 )
/ ID = 7
/ ID = 4
MEDGE( ADD, LSTF, INTE = 50, RATI = 4, 2RAT = 0, PCEN = 0 )

CURVE( SELE, LOCA, WIND = 1 )
/ ID = 10
/ ID = 12
/ ID = 14
/ ID = 15
MEDGE( ADD, LSTF, INTE = 6, RATI = 4, 2RAT = 0, PCEN = 0 )

MEDGE( SELE, LOCA, WIND = 1 )
/ ID = 4
/ ID = 5
/ ID = 6
/ ID = 7
MEDGE( MODI, SUCC, INTE = 6, RATI = 0, 2RAT = 0, PCEN = 0 )

CURVE( SELE, LOCA, WIND = 1 )
```

```
/ ID = 16
CURVE( SELE, LOCA, WIND = 1 )
/ ID = 17
MEDGE( ADD, SUCC, INTE = 6, RATI = 0, 2RAT = 0, PCEN = 0 )

CURVE( SELE, LOCA, WIND = 1 )
/ ID = 1
MEDGE( ADD, SUCC, INTE = 10, RATI = 0, 2RAT = 0, PCEN = 0 )

CURVE( SELE, LOCA, WIND = 1 )
/ ID = 5
/ ID = 2
MEDGE( ADD, SUCC, INTE = 7, RATI = 0, 2RAT = 0, PCEN = 0 )

CURVE( SELE, LOCA, WIND = 1 )
/ ID = 3
/ ID = 6
MEDGE( ADD, SUCC, INTE = 3, RATI = 0, 2RAT = 0, PCEN = 0 )

MEDGE( SELE, LOCA, WIND = 1 )
/ ID = 14
/ ID = 13
MEDGE( MODI, SUCC, INTE = 4, RATI = 0, 2RAT = 0, PCEN = 0 )

CURVE( SELE, LOCA, WIND = 1 )
/ ID = 8
/ ID = 7
/ ID = 16
/ ID = 12
/ ID = 10
/ ID = 17
/ ID = 4
MLOOP( ADD, PAVE )

CURVE( SELE, LOCA, WIND = 1 )
/ ID = 10
/ ID = 12
/ ID = 14
/ ID = 15
MLOOP( ADD, PAVE )

CURVE( SELE, LOCA, WIND = 1 )
/ ID = 17
/ ID = 15
/ ID = 14
/ ID = 16
/ ID = 6
/ ID = 5
/ ID = 1
/ ID = 2
/ ID = 3
MLOOP( ADD, PAVE )
```

```
CURVE( SELE, LOCA, WIND = 1 )
/ ID = 8
/ ID = 7
/ ID = 16
/ ID = 12
/ ID = 10
/ ID = 17
/ ID = 4
MFACE( WIRE, EDG1 = 1, EDG2 = 1, EDG3 = 4, EDG4 = 1 )

CURVE( SELE, LOCA, WIND = 1 )
/ ID = 10
/ ID = 12
/ ID = 14
/ ID = 15
MFACE( WIRE, EDG1 = 1, EDG2 = 1, EDG3 = 1, EDG4 = 1 )

CURVE( SELE, LOCA, WIND = 1 )
/ ID = 17
/ ID = 15
/ ID = 14
/ ID = 16
/ ID = 6
/ ID = 5
/ ID = 1
/ ID = 2
/ ID = 3
MFACE( WIRE, EDG1 = 4, EDG2 = 1, EDG3 = 3, EDG4 = 1 )

POINT( SELE, LOCA, WIND = 1 )
/ ID = 1
/ ID = 13
CURVE( ADD, LINE )

CURVE( SELE, LOCA, WIND = 1 )
/ ID = 18
MEDGE( ADD, SUCC, INTE = 6, RATI = 0, 2RAT = 0, PCEN = 0 )

MFACE( SELE, LOCA, WIND = 1 )
/ ID = 3
/ ID = 18
MSOLID( PROJ )

MFACE( SELE, LOCA, WIND = 1 )
/ ID = 2
CURVE( SELE, LOCA, WIND = 1 )
/ ID = 29
MSOLID( PROJ )

MFACE( SELE, LOCA, WIND = 1 )
/ ID = 1
```

```
CURVE( SELE, LOCA, WIND = 1 )
/ ID = 28
MSOLID( PROJ )


POINT( ADD, SHOW, COOR, X = 0, Y = 13.335, Z = 16.2 )
POINT( ADD, SHOW, COOR, X = 0, Y = 42.545, Z = 16.2 )
POINT( ADD, SHOW, COOR, X = 13.335, Y = 0, Z = 16.2 )
POINT( ADD, SHOW, COOR, X = 13.335, Y = 55.88, Z = 16.2 )
POINT( ADD, SHOW, COOR, X = 23.495, Y = 0, Z = 16.2 )
POINT( ADD, SHOW, COOR, X = 23.495, Y = 55.88, Z = 16.2 )
POINT( ADD, SHOW, COOR, X = 318.135, Y = 0, Z = 16.2 )
POINT( ADD, SHOW, COOR, X = 318.135, Y = 55.88, Z = 16.2 )
POINT( ADD, SHOW, COOR, X = 23.495, Y = 21.2725, Z = 16.2 )
POINT( ADD, SHOW, COOR, X = 30.1625, Y = 27.94, Z = 16.2 )
POINT( ADD, SHOW, COOR, X = 23.495, Y = 34.6075, Z = 16.2 )
POINT( ADD, SHOW, COOR, X = 16.8275, Y = 27.94, Z = 16.2 )


POINT( SELE, LOCA, WIND = 1 )
/ ID = 25
/ ID = 26
CURVE( ADD, LINE )

POINT( SELE, LOCA, WIND = 1 )
/ ID = 25
/ ID = 27
/ ID = 29
/ ID = 31
CURVE( ADD, LINE )

POINT( SELE, LOCA, WIND = 1 )
/ ID = 26
/ ID = 28
/ ID = 30
/ ID = 32
CURVE( ADD, LINE )

POINT( SELE, LOCA, WIND = 1 )
/ ID = 31
/ ID = 32
CURVE( ADD, LINE )

POINT( SELE, LOCA, WIND = 1 )
/ ID = 24
/ ID = 31
CURVE( ADD, LINE )

POINT( SELE, LOCA, WIND = 1 )
/ ID = 23
/ ID = 32
CURVE( ADD, LINE )
```

```
POINT( SELE, LOCA, WIND = 1 )
/ ID = 21
/ ID = 29
CURVE( ADD, LINE )

POINT( SELE, LOCA, WIND = 1 )
/ ID = 20
/ ID = 27
CURVE( ADD, LINE )

POINT( SELE, LOCA, WIND = 1 )
/ ID = 13
/ ID = 25
CURVE( ADD, LINE )

POINT( SELE, LOCA, WIND = 1 )
/ ID = 19
/ ID = 26
CURVE( ADD, LINE )

POINT( SELE, LOCA, WIND = 1 )
/ ID = 18
/ ID = 28
CURVE( ADD, LINE )

POINT( SELE, LOCA, WIND = 1 )
/ ID = 17
/ ID = 30
CURVE( ADD, LINE )

POINT( SELE, LOCA, WIND = 1 )
/ ID = 33
/ ID = 34
/ ID = 35
CURVE( ADD, CIRC )

CURVE( SELE, LOCA, WIND = 1 )
/ ID = 60
POINT( SELE, LOCA, WIND = 1 )
/ ID = 34
CURVE( SPLI )

CURVE( SELE, LOCA, WIND = 1 )
/ ID = 62
POINT( SELE, LOCA, WIND = 1 )
/ ID = 35
CURVE( SPLI )

CURVE( SELE, LOCA, WIND = 1 )
/ ID = 64
POINT( SELE, LOCA, WIND = 1 )
```

```
/ ID = 36
CURVE( SPLI )

POINT( SELE, LOCA, WIND = 1 )
/ ID = 29
/ ID = 33
CURVE( ADD, LINE )

POINT( SELE, LOCA, WIND = 1 )
/ ID = 30
/ ID = 35
CURVE( ADD, LINE )

POINT( SELE, LOCA, WIND = 1 )
/ ID = 14
/ ID = 33
CURVE( ADD, LINE )

POINT( SELE, LOCA, WIND = 1 )
/ ID = 22
/ ID = 34
CURVE( ADD, LINE )

POINT( SELE, LOCA, WIND = 1 )
/ ID = 16
/ ID = 35
CURVE( ADD, LINE )

POINT( SELE, LOCA, WIND = 1 )
/ ID = 15
/ ID = 36
CURVE( ADD, LINE )

CURVE( SELE, LOCA, WIND = 1 )
/ ID = 44
MEDGE( ADD, SUCC, INTE = 10, RATI = 0, 2RAT = 0, PCEN = 0 )

CURVE( SELE, LOCA, WIND = 1 )
/ ID = 45
/ ID = 48
MEDGE( ADD, SUCC, INTE = 7, RATI = 0, 2RAT = 0, PCEN = 0 )

CURVE( SELE, LOCA, WIND = 1 )
/ ID = 46
/ ID = 49
MEDGE( ADD, SUCC, INTE = 4, RATI = 0, 2RAT = 0, PCEN = 0 )

CURVE( SELE, LOCA, WIND = 1 )
/ ID = 67
/ ID = 66
/ ID = 65
/ ID = 63
```

```
/ ID = 61
/ ID = 68
MEDGE( ADD, SUCC, INTE = 6, RATI = 0, 2RAT = 0, PCEN = 0 )

CURVE( SELE, LOCA, WIND = 1 )
/ ID = 54
/ ID = 55
/ ID = 56
/ ID = 57
/ ID = 58
/ ID = 59
/ ID = 71
/ ID = 72
/ ID = 69
/ ID = 70
MEDGE( ADD, SUCC, INTE = 3, RATI = 0, 2RAT = 0, PCEN = 0 )

CURVE( SELE, LOCA, WIND = 1 )
/ ID = 51
MEDGE( ADD, SUCC, INTE = 24, RATI = 0, 2RAT = 0, PCEN = 0 )

CURVE( SELE, LOCA, WIND = 1 )
/ ID = 47
/ ID = 50
MEDGE( ADD, LSTF, INTE = 50, RATI = 4, 2RAT = 0, PCEN = 0 )

CURVE( SELE, LOCA, WIND = 1 )
/ ID = 52
/ ID = 53
MEDGE( ADD, SUCC, INTE = 3, RATI = 0, 2RAT = 0, PCEN = 0 )

CURVE( SELE, LOCA, WIND = 1 )
/ ID = 67
/ ID = 66
/ ID = 65
/ ID = 68
/ ID = 49
/ ID = 48
/ ID = 44
/ ID = 45
/ ID = 46
MLOOP( ADD, PAVE )

CURVE( SELE, LOCA, WIND = 1 )
/ ID = 67
/ ID = 69
/ ID = 19
/ ID = 54
MLOOP( ADD, PAVE )

CURVE( SELE, LOCA, WIND = 1 )
/ ID = 66
```

/ ID = 72
/ ID = 20
/ ID = 69
MLOOP(ADD, PAVE)

CURVE(SELE, LOCA, WIND = 1)
/ ID = 65
/ ID = 71
/ ID = 21
/ ID = 72
MLOOP(ADD, PAVE)

CURVE(SELE, LOCA, WIND = 1)
/ ID = 68
/ ID = 59
/ ID = 22
/ ID = 71
MLOOP(ADD, PAVE)

CURVE(SELE, LOCA, WIND = 1)
/ ID = 49
/ ID = 58
/ ID = 23
/ ID = 59
MLOOP(ADD, PAVE)

CURVE(SELE, LOCA, WIND = 1)
/ ID = 48
/ ID = 57
/ ID = 24
/ ID = 58
MLOOP(ADD, PAVE)

CURVE(SELE, LOCA, WIND = 1)
/ ID = 44
/ ID = 56
/ ID = 25
/ ID = 57
MLOOP(ADD, PAVE)

CURVE(SELE, LOCA, WIND = 1)
/ ID = 45
/ ID = 55
/ ID = 26
/ ID = 56
MLOOP(ADD, PAVE)

CURVE(SELE, LOCA, WIND = 1)
/ ID = 46
/ ID = 54
/ ID = 27
/ ID = 55

```
MLOOP( ADD, PAVE )

CURVE( SELE, LOCA, WIND = 1 )
/ ID = 67
/ ID = 66
/ ID = 65
/ ID = 68
/ ID = 49
/ ID = 48
/ ID = 44
/ ID = 45
/ ID = 46
MFACE( WIRE, EDG1 = 4, EDG2 = 1, EDG3 = 3, EDG4 = 1 )

CURVE( SELE, LOCA, WIND = 1 )
/ ID = 67
/ ID = 69
/ ID = 19
/ ID = 54
MFACE( WIRE, EDG1 = 1, EDG2 = 1, EDG3 = 1, EDG4 = 1 )

CURVE( SELE, LOCA, WIND = 1 )
/ ID = 66
/ ID = 72
/ ID = 20
/ ID = 69
MFACE( WIRE, EDG1 = 1, EDG2 = 1, EDG3 = 1, EDG4 = 1 )

CURVE( SELE, LOCA, WIND = 1 )
/ ID = 65
/ ID = 71
/ ID = 21
/ ID = 72
MFACE( WIRE, EDG1 = 1, EDG2 = 1, EDG3 = 1, EDG4 = 1 )

CURVE( SELE, LOCA, WIND = 1 )
/ ID = 68
/ ID = 59
/ ID = 22
/ ID = 71
MFACE( WIRE, EDG1 = 1, EDG2 = 1, EDG3 = 1, EDG4 = 1 )

CURVE( SELE, LOCA, WIND = 1 )
/ ID = 49
/ ID = 58
/ ID = 23
/ ID = 59
MFACE( WIRE, EDG1 = 1, EDG2 = 1, EDG3 = 1, EDG4 = 1 )

CURVE( SELE, LOCA, WIND = 1 )
/ ID = 48
/ ID = 57
```

```
/ ID = 24
/ ID = 58
MFACE( WIRE, EDG1 = 1, EDG2 = 1, EDG3 = 1, EDG4 = 1 )

CURVE( SELE, LOCA, WIND = 1 )
/ ID = 44
/ ID = 56
/ ID = 25
/ ID = 57
MFACE( WIRE, EDG1 = 1, EDG2 = 1, EDG3 = 1, EDG4 = 1 )

CURVE( SELE, LOCA, WIND = 1 )
/ ID = 45
/ ID = 55
/ ID = 26
/ ID = 56
MFACE( WIRE, EDG1 = 1, EDG2 = 1, EDG3 = 1, EDG4 = 1 )

CURVE( SELE, LOCA, WIND = 1 )
/ ID = 46
/ ID = 54
/ ID = 27
/ ID = 55
MFACE( WIRE, EDG1 = 1, EDG2 = 1, EDG3 = 1, EDG4 = 1 )

MFACE( SELE, LOCA, WIND = 1 )
/ ID = 21
/ ID = 4
/ ID = 22
/ ID = 23
/ ID = 24
/ ID = 25
/ ID = 26
/ ID = 27
/ ID = 28
/ ID = 29
/ ID = 30
MSHELL( ADD, VISI, NOSH )

MSHELL( SELE, LOCA, WIND = 1 )
/ ID = 4
MSOLID( ADD, MAP )


CURVE( SELE, LOCA, WIND = 1 )
/ ID = 63
/ ID = 65
/ ID = 66
/ ID = 61
MLOOP( ADD, PAVE )

CURVE( SELE, LOCA, WIND = 1 )
```

```
/ ID = 63
/ ID = 70
/ ID = 37
/ ID = 71
MLOOP( ADD, PAVE )

CURVE( SELE, LOCA, WIND = 1 )
/ ID = 61
/ ID = 69
/ ID = 36
/ ID = 70
MLOOP( ADD, PAVE )

CURVE( SELE, LOCA, WIND = 1 )
/ ID = 63
/ ID = 65
/ ID = 66
/ ID = 61
MFACE( WIRE, EDG1 = 1, EDG2 = 1, EDG3 = 1, EDG4 = 1 )

CURVE( SELE, LOCA, WIND = 1 )
/ ID = 63
/ ID = 70
/ ID = 37
/ ID = 71
MFACE( WIRE, EDG1 = 1, EDG2 = 1, EDG3 = 1, EDG4 = 1 )

CURVE( SELE, LOCA, WIND = 1 )
/ ID = 61
/ ID = 69
/ ID = 36
/ ID = 70
MFACE( WIRE, EDG1 = 1, EDG2 = 1, EDG3 = 1, EDG4 = 1 )

MFACE( SELE, LOCA, WIND = 1 )
/ ID = 31
/ ID = 14
/ ID = 32
/ ID = 24
/ ID = 23
/ ID = 33
MSHELL( ADD, VISI, NOSH )

MSHELL( SELE, LOCA, WIND = 1 )
MSOLID( ADD, MAP )

CURVE( SELE, LOCA, WIND = 1 )
/ ID = 51
/ ID = 50
/ ID = 68
/ ID = 63
/ ID = 61
```

```
/ ID = 67
/ ID = 47
MLOOP( ADD, PAVE )

CURVE( SELE, LOCA, WIND = 1 )
/ ID = 47
/ ID = 52
/ ID = 41
/ ID = 54
MLOOP( ADD, PAVE )

CURVE( SELE, LOCA, WIND = 1 )
/ ID = 51
/ ID = 53
/ ID = 39
/ ID = 52
MLOOP( ADD, PAVE )

CURVE( SELE, LOCA, WIND = 1 )
/ ID = 50
/ ID = 59
/ ID = 40
/ ID = 53
MLOOP( ADD, PAVE )

CURVE( SELE, LOCA, WIND = 1 )
/ ID = 51
/ ID = 50
/ ID = 68
/ ID = 63
/ ID = 61
/ ID = 67
/ ID = 47
MFACE( WIRE, EDG1 = 1, EDG2 = 1, EDG3 = 4, EDG4 = 1 )

CURVE( SELE, LOCA, WIND = 1 )
/ ID = 47
/ ID = 52
/ ID = 41
/ ID = 54
MFACE( WIRE, EDG1 = 1, EDG2 = 1, EDG3 = 1, EDG4 = 1 )

CURVE( SELE, LOCA, WIND = 1 )
/ ID = 51
/ ID = 53
/ ID = 39
/ ID = 52
MFACE( WIRE, EDG1 = 1, EDG2 = 1, EDG3 = 1, EDG4 = 1 )

CURVE( SELE, LOCA, WIND = 1 )
/ ID = 50
/ ID = 59
```

/ ID = 40
/ ID = 53
MFACE(WIRE, EDG1 = 1, EDG2 = 1, EDG3 = 1, EDG4 = 1)

MFACE(SELE, LOCA, WIND = 1)
/ ID = 34
/ ID = 17
/ ID = 35
/ ID = 36
/ ID = 37
/ ID = 25
/ ID = 32
/ ID = 33
/ ID = 22
MSHELL(ADD, VISI, NOSH)

MSHELL(SELE, ID = 6)
MSOLID(ADD, MAP)

POINT(ADD, SHOW, COOR, X = 0, Y = 13.335, Z = 40.64)

POINT(SELE, LOCA, WIND = 1)
/ ID = 25
/ ID = 37
CURVE(ADD, LINE)

CURVE(SELE, LOCA, WIND = 1)
/ ID = 73
MEDGE(ADD, SUCC, INTE = 12, RATI = 0, 2RAT = 0, PCEN = 0)

MFACE(SELE, LOCA, WIND = 1)
/ ID = 21
CURVE(SELE, LOCA, WIND = 1)
/ ID = 73
MSOLID(PROJ)

MFACE(SELE, LOCA, WIND = 1)
/ ID = 31
CURVE(SELE, LOCA, WIND = 1)
/ ID = 84
MSOLID(PROJ)

MFACE(SELE, LOCA, WIND = 1)
/ ID = 34
CURVE(SELE, LOCA, WIND = 1)
/ ID = 83
MSOLID(PROJ)

POINT(ADD, SHOW, COOR, X = 23.495, Y = 21.2725, Z = 80)

POINT(SELE, LOCA, WIND = 1)

```
/ ID = 38
/ ID = 49
CURVE( ADD, LINE )

CURVE( SELE, LOCA, WIND = 1 )
/ ID = 99
MEDGE( ADD, SUCC, INTE = 18, RATI = 0, 2RAT = 0, PCEN = 0 )

MFACE( SELE, LOCA, WIND = 1 )
/ ID = 48
CURVE( SELE, LOCA, WIND = 1 )
/ ID = 99
MSOLID( PROJ )

MFAC = 1, BEDG = 1, SPAV = 1, MSHE = 1, MSOL = 1, COOR = 1 )
MSOLID( SELE, ID = 1 )
ELEMENT( SETD, BRIC, NODE = 8 )
MSOLID( MESH, MAP, ENTI = “1”, ALG1 )
MSOLID( SELE, ID = 2 )
MSOLID( MESH, MAP, ENTI = “2”, ALG1 )
MSOLID( SELE, ID = 3 )
MSOLID( MESH, MAP, ENTI = “3”, ALG1 )
MSOLID( SELE, ID = 4 )
MSOLID( MESH, MAP, ENTI = “4”, ALG1 )
MSOLID( SELE, ID = 5 )
MSOLID( MESH, MAP, ENTI = “5”, ALG1 )
MSOLID( SELE, ID = 6 )
MSOLID( MESH, MAP, ENTI = “6”, ALG1 )
MSOLID( SELE, ID = 7 )
MSOLID( MESH, MAP, ENTI = “7”, ALG1 )
MSOLID( SELE, ID = 8 )
MSOLID( MESH, MAP, ENTI = “8”, ALG1 )
MSOLID( SELE, ID = 9 )
MSOLID( MESH, MAP, ENTI = “9”, ALG1 )
MSOLID( SELE, ID = 10 )
MSOLID( MESH, MAP, ENTI = “10”, ALG1 )
END(  )
```

C.2 Boundary Conditions Defined in FI-BC

```
FI-BC(  )
BGADD( SELE, FACE, INCL, LOCA, WIND = 1 )
/ ID = 52
/ ID = 35
/ ID = 17
BGADD( ADD, FACE, ENTI = “inlet”, INCL )

BGADD( SELE, FACE, INCL, LOCA, WIND = 1 )
/ ID = 51
/ ID = 34
/ ID = 16
BGADD( ADD, FACE, ENTI = “wall”, INCL )
```

```
BGADD( SELE, FACE, INCL, LOCA, WIND = 1 )
/ ID = 38
/ ID = 21
/ ID = 1
BGADD( ADD, FACE, ENTI = “wall”, INCL )

BGADD( SELE, FACE, INCL, LOCA, WIND = 1 )
/ ID = 40
/ ID = 23
/ ID = 4
BGADD( ADD, FACE, ENTI = “wall”, INCL )

BGADD( SELE, FACE, INCL, LOCA, WIND = 1 )
/ ID = 41
/ ID = 24
/ ID = 5
BGADD( ADD, FACE, ENTI = “wall”, INCL )

BGADD( SELE, FACE, INCL, LOCA, WIND = 1 )
/ ID = 42
/ ID = 25
/ ID = 6
BGADD( ADD, FACE, ENTI = “wall”, INCL )

BGADD( SELE, FACE, INCL, LOCA, WIND = 1 )
/ ID = 43
/ ID = 26
/ ID = 7
BGADD( ADD, FACE, ENTI = “wall”, INCL )

BGADD( SELE, FACE, INCL, LOCA, WIND = 1 )
/ ID = 53
/ ID = 36
/ ID = 19
BGADD( ADD, FACE, ENTI = “wall”, INCL )

BGADD( SELE, FACE, INCL, LOCA, WIND = 1 )
/ ID = 18
/ ID = 3
BGADD( ADD, FACE, ENTI = “wall”, INCL )

BGADD( SELE, FACE, INCL, LOCA, WIND = 1 )
/ ID = 13
BGADD( ADD, FACE, ENTI = “wall”, INCL )

BGADD( SELE, FACE, INCL, LOCA, WIND = 1 )
/ ID = 54
/ ID = 47
BGADD( ADD, FACE, ENTI = “wall2”, INCL )

BGADD( SELE, FACE, INCL, LOCA, WIND = 1 )
```

/ ID = 15
BGADD(ADD, FACE, ENTI = “intake”, INCL)

BGADD(SELE, FACE, INCL, LOCA, WIND = 1)
/ ID = 29
/ ID = 28
BGADD(ADD, FACE, ENTI = “bell1”, INCL)

BGADD(SELE, FACE, INCL, LOCA, WIND = 1)
/ ID = 32
/ ID = 31
BGADD(ADD, FACE, ENTI = “bell2”, INCL)

BGADD(SELE, FACE, INCL, LOCA, WIND = 1)
/ ID = 46
/ ID = 45
BGADD(ADD, FACE, ENTI = “pipe1”, INCL)

BGADD(SELE, FACE, INCL, LOCA, WIND = 1)
/ ID = 49
/ ID = 48
BGADD(ADD, FACE, ENTI = “pipe2”, INCL)

BGADD(SELE, FACE, INCL, LOCA, WIND = 1)
/ ID = 33
BGADD(ADD, FACE, ENTI = “mid1”, INCL)

BGADD(SELE, FACE, INCL, LOCA, WIND = 1)
/ ID = 50
BGADD(ADD, FACE, ENTI = “mid2”, INCL)

BGADD(SELE, FACE, INCL, LOCA, WIND = 1)
/ ID = 58
/ ID = 56
/ ID = 55
BGADD(ADD, FACE, ENTI = “cylinder”, INCL)

BGADD(SELE, FACE, INCL, LOCA, WIND = 1)
/ ID = 59
BGADD(ADD, FACE, ENTI = “outlet”, INCL)

BCSENTITY(BCNO)
BCSENTITY(SELE, NAME = “inlet”)
BCNODE(UX, GSEL, CONS = -8.65)
BCNODE(UY, GSEL, ZERO)
BCNODE(UZ, GSEL, ZERO)
UTILITY(UNSE, ALL)
BCSENTITY(SELE, NAME = “wall”)
BCSENTITY(SELE, NAME = “wall2”)
BCSENTITY(SELE, NAME = “bell1”)
BCSENTITY(SELE, NAME = “bell2”)

```
BCSENTITY( SELE, NAME = “pipe1” )
BCSENTITY( SELE, NAME = “pipe2” )
BCSENTITY( SELE, NAME = “cylinder” )
BCNODE( VELO, GSEL, ZERO )
END( )
```

C.3 Solution Method Definition Using FI-PREP

```
FIPREP( )
DATAPRINT( ADD, CONT )
EXECUTION( ADD, NEWJ )
OPTIONS( ADD, UPWI )
PRINTOUT( ADD, NONE, BOUN )
PROBLEM( ADD, 3-D, INCO, STEA, TURB, NONL, NEWT, MOME, ISOT, FIXE, SING )
RELAXATION( ADD )
SOLUTION( ADD, SEGR = 1000, CGS = 0, CR = 0, NCGC = 1e-06, SCGC = 1e-06,
PREC = 21, ACCF = 0.4, PPRO )
ENTITY( ADD, NAME = 1, FLUI )
ENTITY( ADD, NAME = 2, FLUI )
ENTITY( ADD, NAME = 3, FLUI )
ENTITY( ADD, NAME = 4, FLUI )
ENTITY( ADD, NAME = 5, FLUI )
ENTITY( ADD, NAME = 6, FLUI )
ENTITY( ADD, NAME = 7, FLUI )
ENTITY( ADD, NAME = 8, FLUI )
ENTITY( ADD, NAME = 9, FLUI )
ENTITY( ADD, NAME = 10, FLUI )
ENTITY( ADD, NAME = “inlet”, PLOT )
ENTITY( ADD, NAME = “wall”, SLIP )
ENTITY( ADD, NAME = “wall2”, WALL )
ENTITY( ADD, NAME = “cylinder”, WALL )
ENTITY( ADD, NAME = “outlet”, PLOT )
ENTITY( PLOT, NAME = “intake”, ATTA = “2”, NATT = “5” )
ENTITY( WALL, NAME = “bell1”, ATTA = “4”, NATT = “5” )
ENTITY( WALL, NAME = “bell2”, ATTA = “5”, NATT = “6” )
ENTITY( WALL, NAME = “pipe1”, ATTA = “7”, NATT = “8” )
ENTITY( WALL, NAME = “pipe2”, ATTA = “8”, NATT = “9” )
ENTITY( PLOT, NAME = “mid1”, ATTA = “5”, NATT = “8” )
ENTITY( PLOT, NAME = “mid2”, ATTA = “8”, NATT = “10” )
DENSITY( ADD, SET = 1, CONS = 1 )
VISCOSITY( ADD, SET = 1, CONS = 0.01, TWO- )
END( )


CREATE( FISO )
RUN( FISOLV, IDEN = “8-65c”, BACK, AT = “”, TIME = “NOW”, FISOLVME = 9000000,
COMP )
```

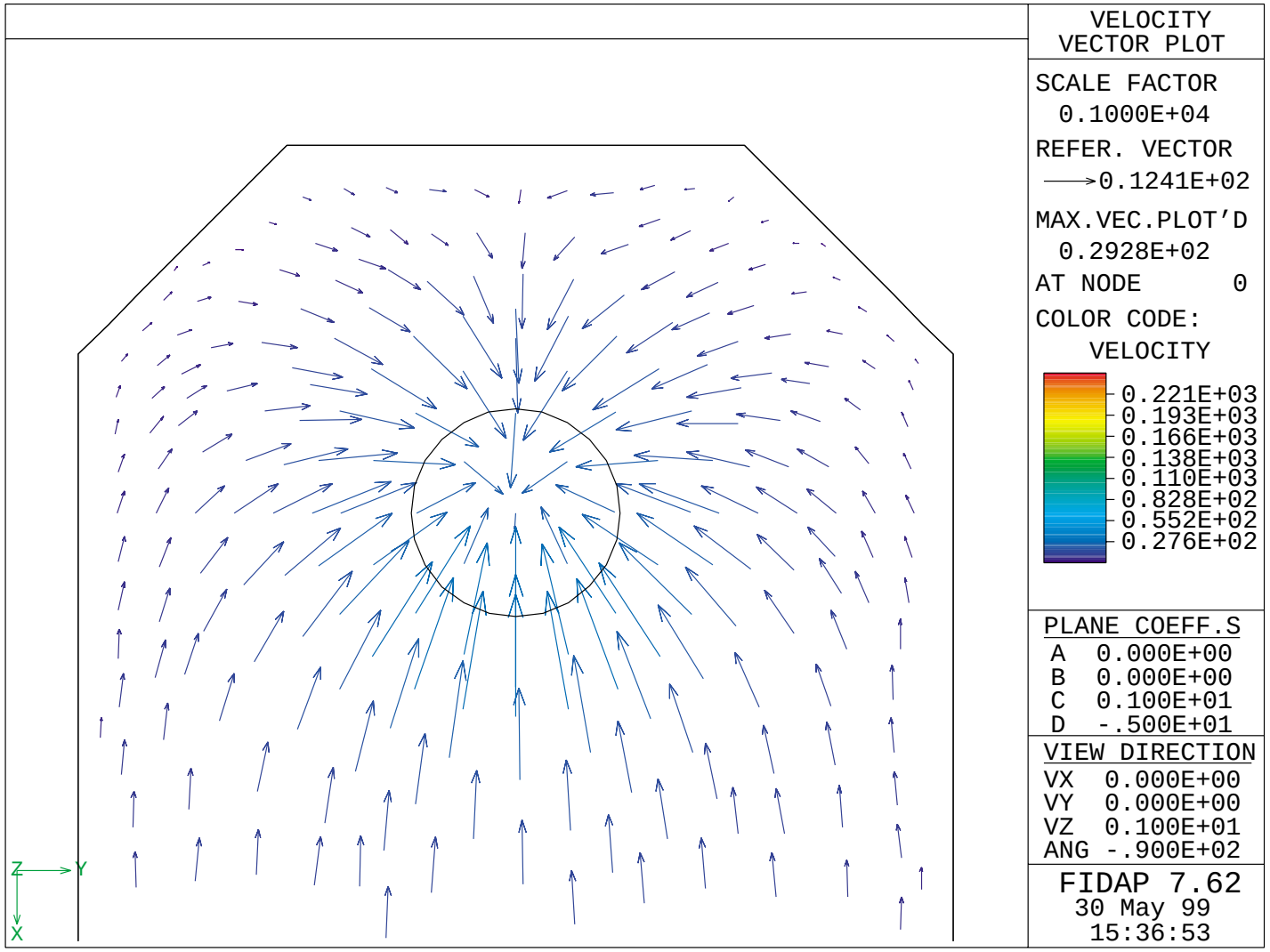

Figure D-1: Velocity Vector Plot - Base Case (Re = 3.6 x 10^4) Plan View Taken at a Depth of 5 cm from the Tank Bottom

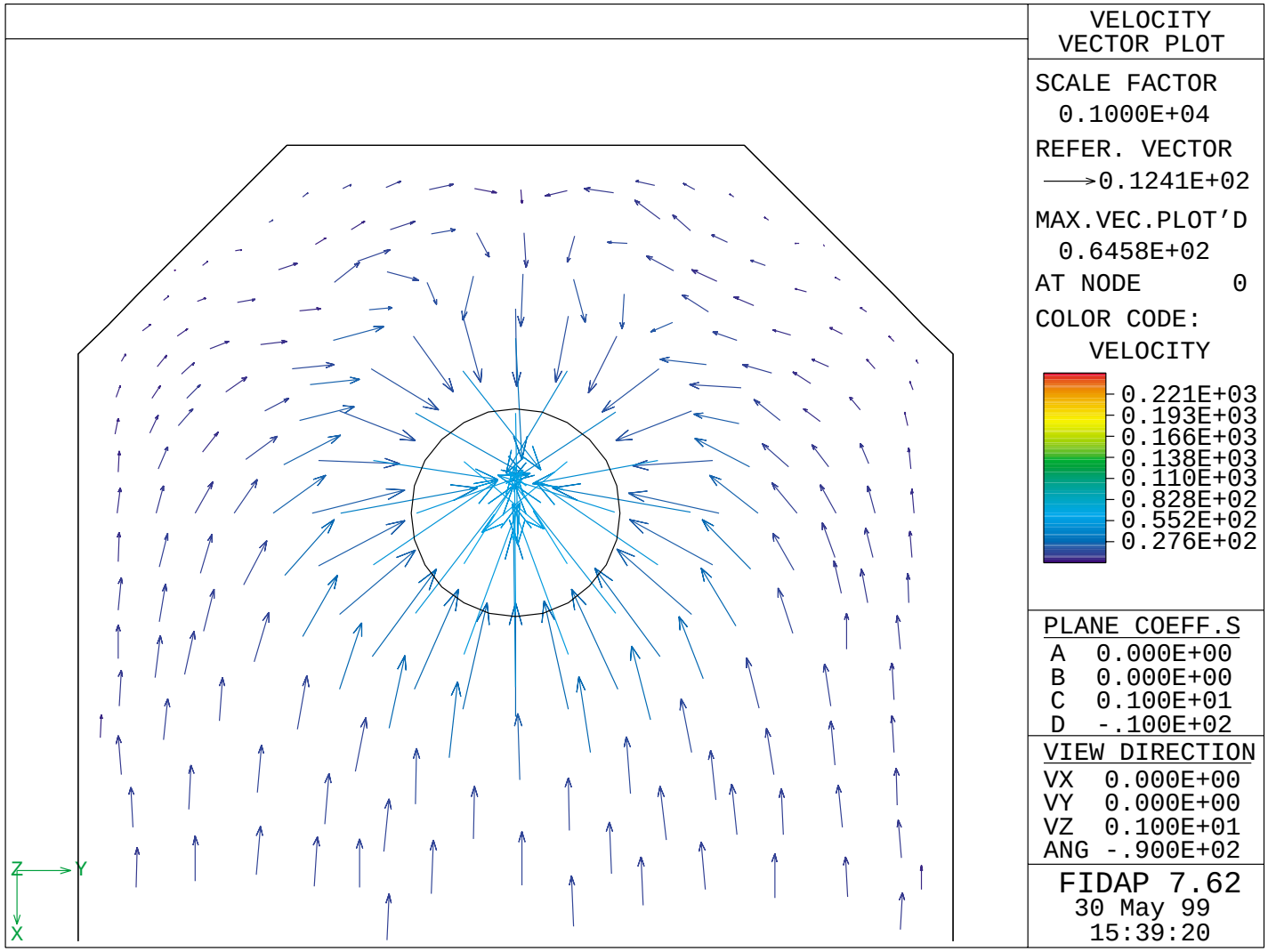

Figure D-2: Velocity Vector Plot - Base Case (Re = 3.6 x 10^4) Plan View Taken at a Depth of 10 cm from the Tank Bottom

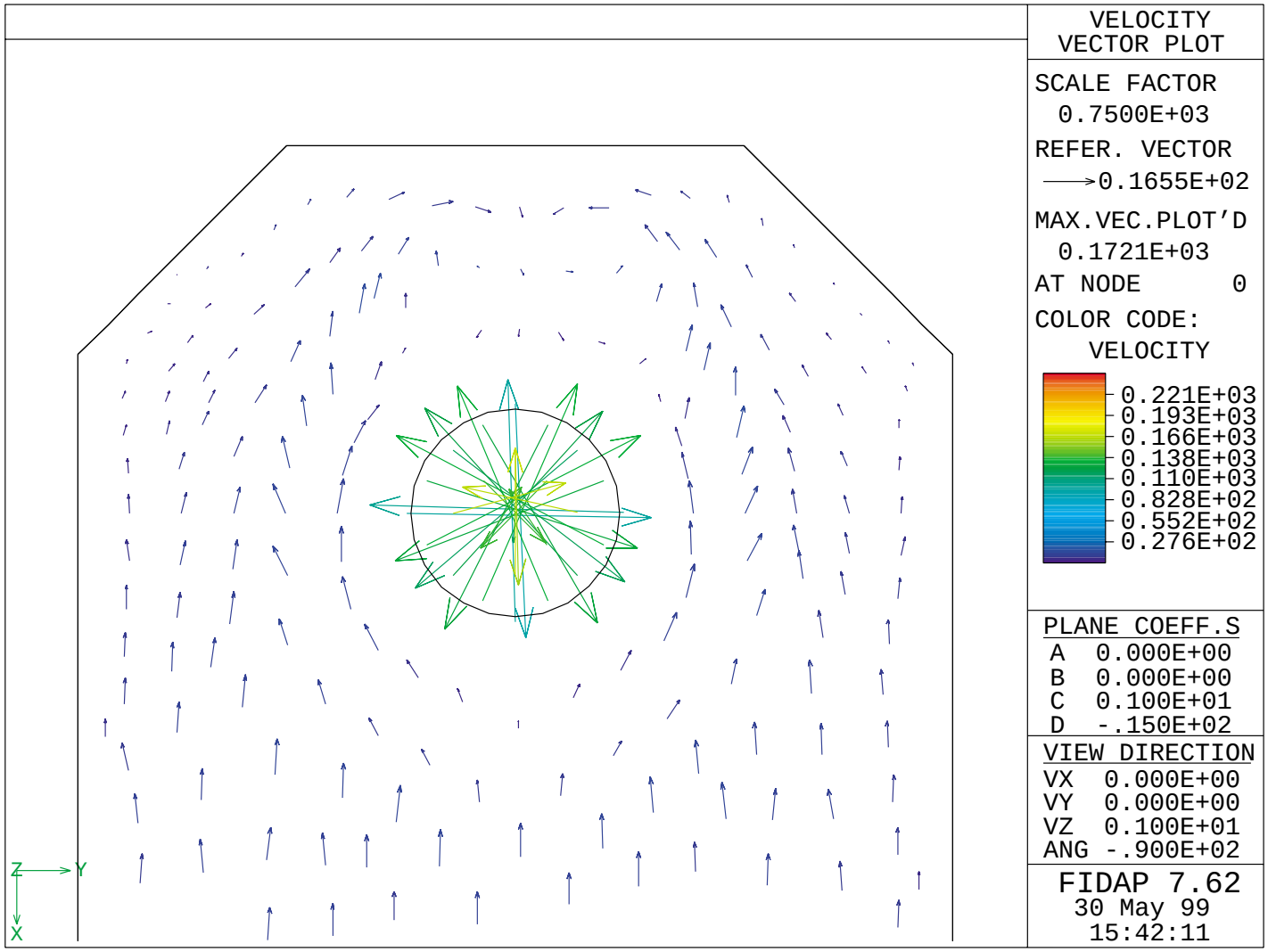

Figure D-3: Velocity Vector Plot - Base Case (Re = 3.6 x 10^4) Plan View Taken at a Depth of 15 cm from the Tank Bottom

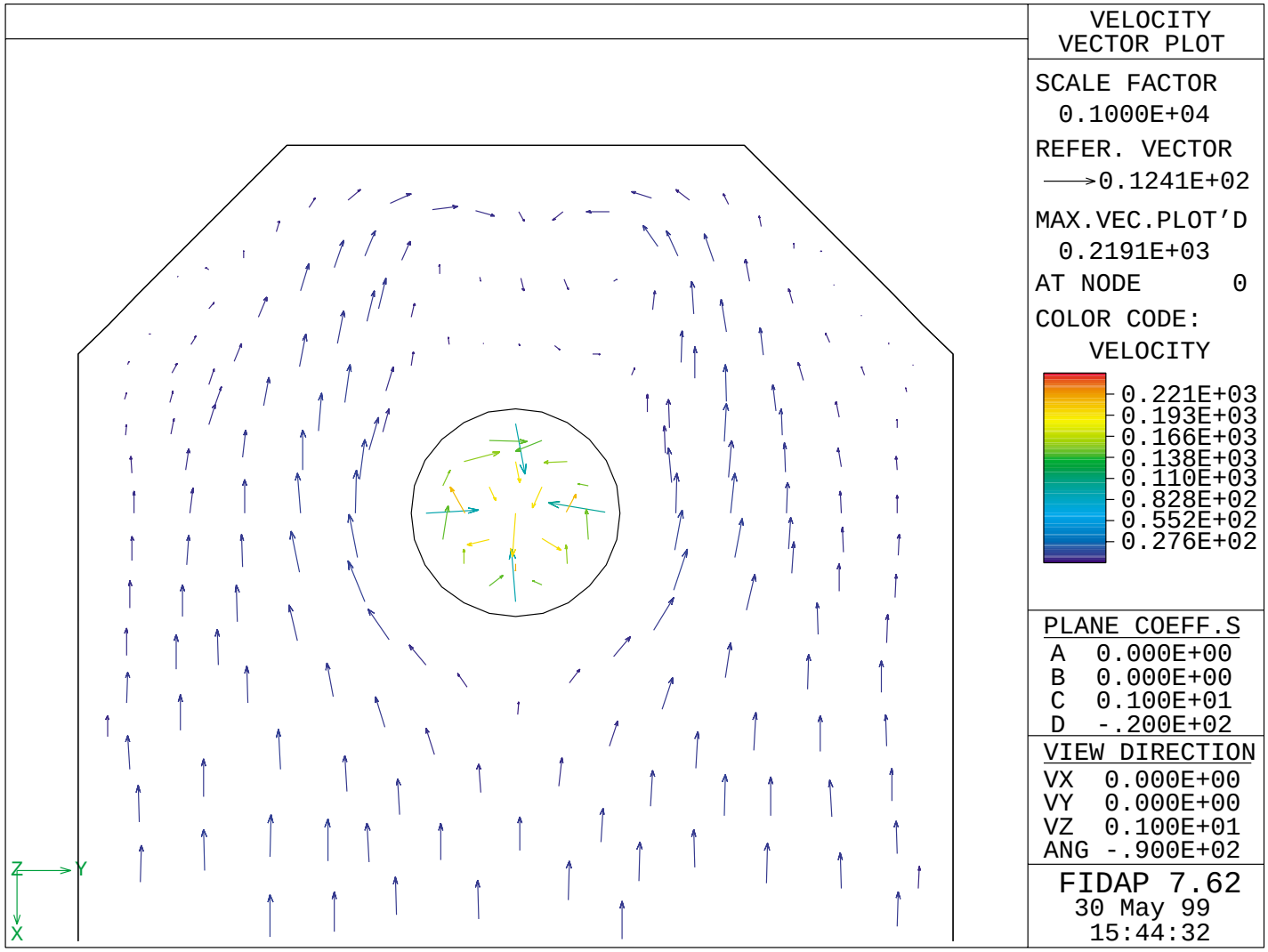

Figure D-4: Velocity Vector Plot - Base Case (Re = 3.6 x 10^4) Plan View Taken at a Depth of 20 cm from the Tank Bottom

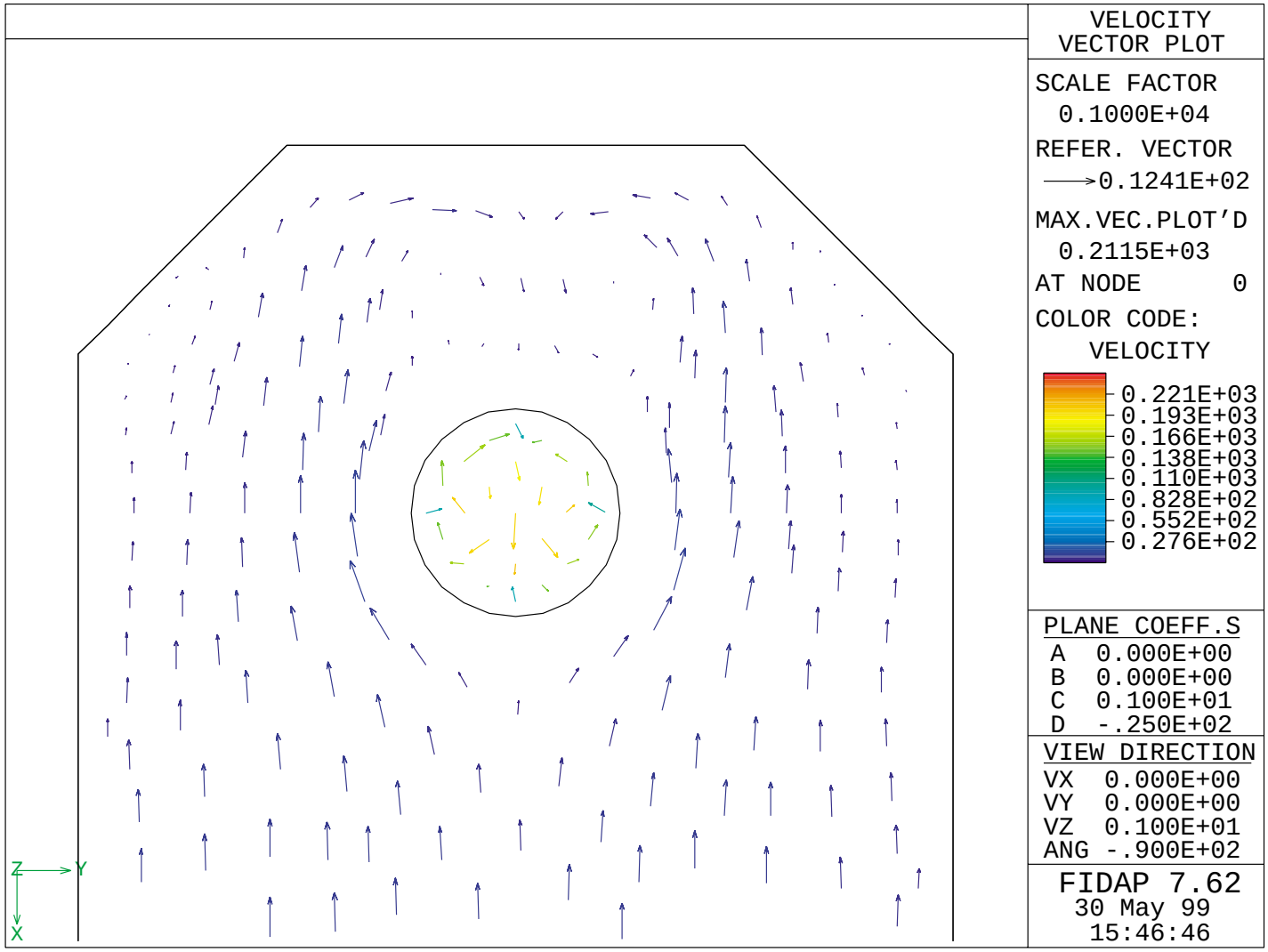

Figure D-5: Velocity Vector Plot - Base Case (Re = 3.6 x 10^4) Plan View Taken at a Depth of 25 cm from the Tank Bottom

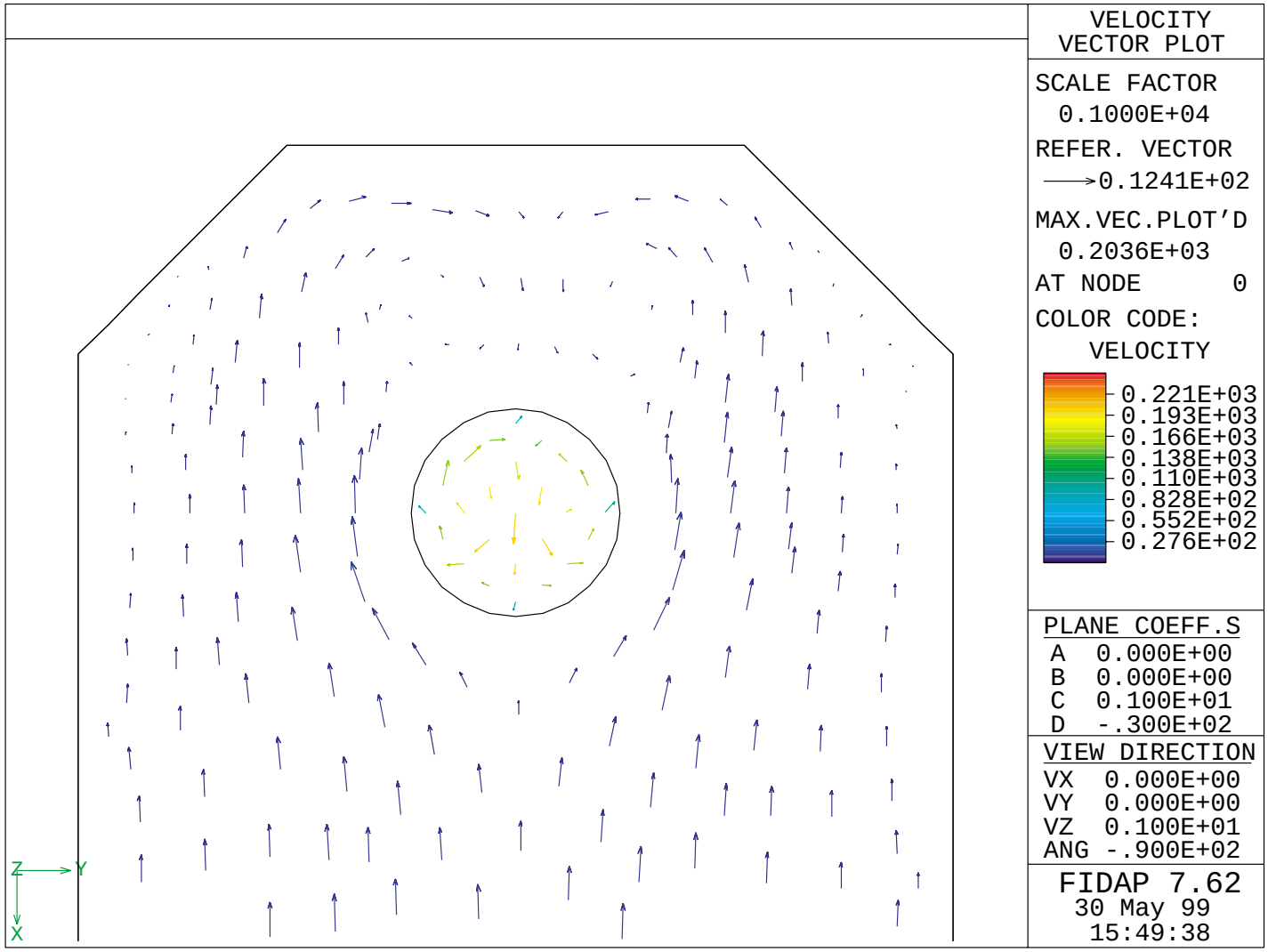

Figure D-6: Velocity Vector Plot - Base Case (Re = 3.6 x 10^4) Plan View Taken at a Depth of 30 cm from the Tank Bottom

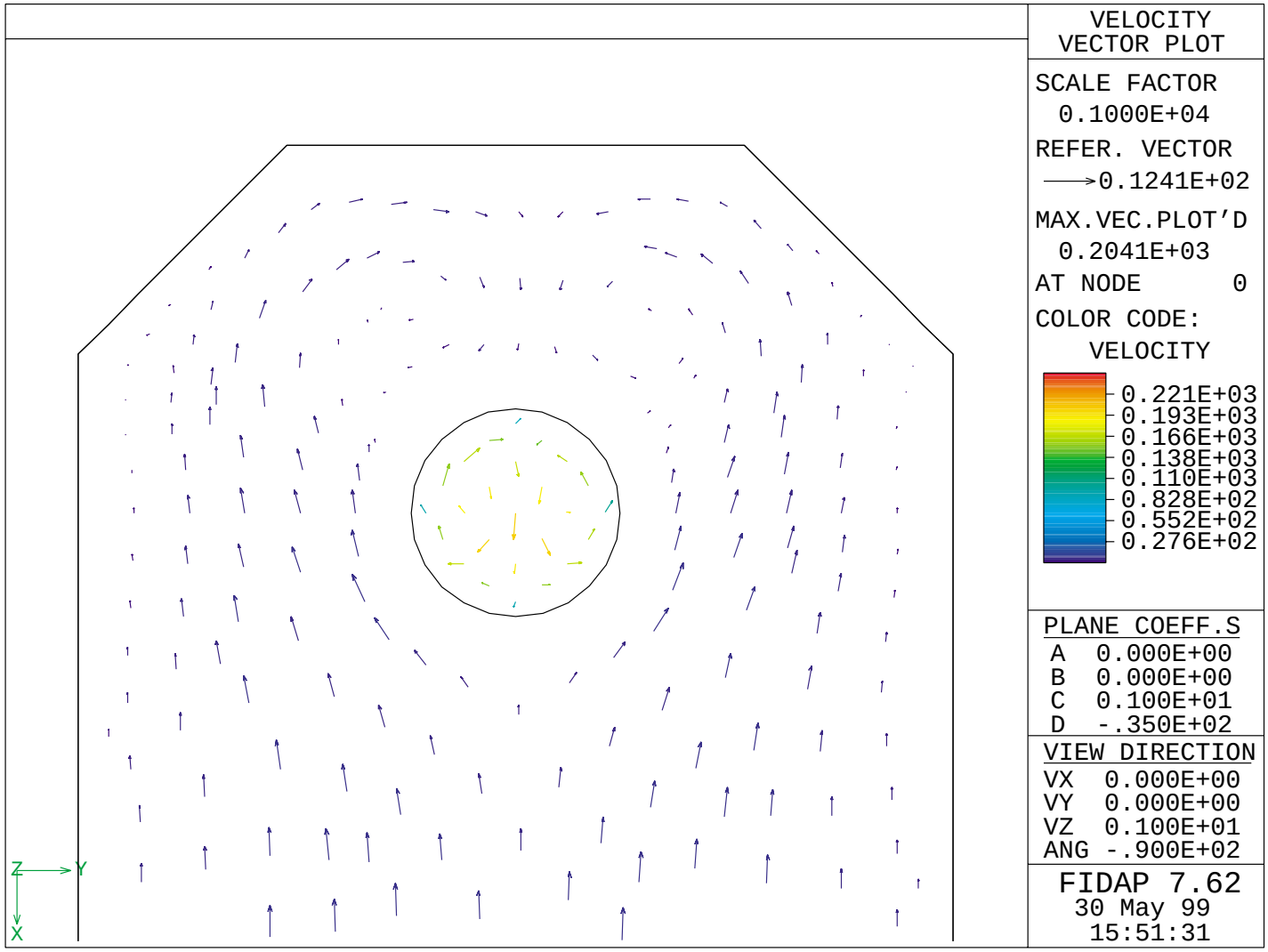

Figure D-7: Velocity Vector Plot - Base Case (Re = 3.6 x 10^4) Plan View Taken at a Depth of 35 cm from the Tank Bottom

References

Constantinescu, G.S. and V.C. Patel, 1997, Role of turbulence model in prediction of pump intake vortices, 10th International Conference on Numerical Methods, Swansea, UK.

Constantinescu, G.S., and V.C. Patel, 1998, "Numerical model for simulation of pump-intake flow and vortices", *Journal of Hydraulic Engineering*, Vol. 124, No. 2, Pp 123-134.

Fluid Dynamics International (FIDAP), 1993a, *FIDAP 7.0 Theory Manual*. Fluent, Inc., Lebanon, NH.

Fluid Dynamics International (FIDAP), 1993b, *FIDAP 7.0 FIMESH Users Manual*, Fluent, Inc., Lebanon, NH.

Fluid Dynamics International (FIDAP), 1993c, *FIPREP 7.0 Users Manual*. Fluent, Inc., Lebanon, NH.

Fluid Dynamics International (FIDAP), 1995, *FIDAP 7.5 Update Manual*. Fluent, Inc., Lebanon, NH.

Fluid Dynamics International (FIDAP), 1996, *FIDAP 7.6 Update Manual*, Fluent, Inc., Lebanon, NH.

Hecker, G. E., 1984, "Scale effects in modeling vortices" *Symposium on Scale Effects in Modeling Hydraulic Structures*, International Association for Hydraulic Research.

Hydraulic Institute, 1975, *Hydraulic Institute standards for centrifugal, rotary, and reciprocating pumps*, 13th edition, Cleveland, Ohio.

Launder, B.E., 1990, "Modeling the formation and dispersal of streamwise vortices in turbulent flow", *The Aeronautical Journal*, Vol. 99, No 990, Pp 419.

Levi, E., 1972, "Experiments on unstable vortices" *Journal of the Engineering Mechanics Division*, ASCE, Vol 98, No EM3, Pp 539-559.

Padmanabhan, M. and G.E. Hecker, 1984, "Scale effects in pump sump models," J. Hydr. Div., ASCE, 110(11), Pp 1540-1556.

Rood, E. P., 1994, "Interpreting Vortex Interactions with a Free Surface" *Journal of Fluids Engineering*, Vol 116, Pp 91-94.

Rood, Edwin P., 1995, "Vorticity Interactions with a Free Surface" *Fluid Vortices*, Pp 687-730.

Shin, C.S., E.M. Greitzer, W.K. Cheng, C.S. Tan, and C.L. Shippee, 1986, "Circulation measurements and vortical structure in an inlet-vortex field", *Journal of Fluid Mechanics*, Vol 162, Pp 463-487.

Spezial, C.G., 1990, "Analytical methods for the development of Reynolds-stress closures in turbulence" *Annual Review of Fluid Mechanics*, Vol 23, Pp 107-157.

Sweeney, C.E., R.A. Elder, and D. Hay, 1982, "Pump sump design experience: summary", *Journal of the Hydraulics Division*, ASCE, Vol. 108, No. HY3.